Madagascar's burned area from Sentinel-2 imagery (2016–2022): Four times higher than from lower resolution sensors.

Fernández-García, V. [1, 2], Franquesa, M. [3], Kull, C.A.[1]

[1]Institute of Geography and Sustainability, Faculty of Geosciences and Environment, Université de Lausanne, Géopolis, Lausanne, CH-1015, Switzerland.
[2]Ecology, Department of Biodiversity and Environmental Management, Faculty of Biological and Environmental Sciences, Universidad de León, León, 24071, Spain.
[3]Instituto Pirenaico de Ecología, Consejo Superior de Investigaciones Científicas (IPE-CSIC), Zaragoza, 50059, Spain.

Correspondence to: Víctor Fernández-García (victor.fernandezgarcia@unil.ch)

This is an author-archived preprint version of the manuscript "Madagascar's burned area from Sentinel-2 imagery (2016–2022): Four times higher than from lower resolution sensors." Published by *Science of the Total Environment*. Please, cite the manuscript as:

Fernández-García, V., Franquesa, M., Kull, C.A. (2024). Madagascar's burned area from Sentinel-2 imagery (2016–2022): Four times higher than from lower resolution sensors. *Science of the Total Environment* 914, 169929. https://doi.org/10.1016/j.scitotenv.2024.169929

Abstract. Madagascar is one of the most burned regions in the world, to the point that it has been called the 'Isle of fire' or the 'Burning Island'. An accurate characterization of the burned area (BA) is crucial for understanding the true situation and impacts of fires on this island, where there is an active scientific debate on how fire affects multiple environmental and socioeconomic aspects, and how fire regimes should be in a complex context with differing interests. Despite this, recent advances have revealed that BA in Madagascar is poorly characterised by the currently available global BA products. In this work, we present, validate, and explore a BA database at 20 m spatial resolution for Madagascar covering the period 2016-2022. The database was built based on 75,010 Sentinel-2 images using a two-phase BA detection algorithm. The validation with independent long-term reference units showed Dice coefficients ≥79%, omission errors ≤24%, commission errors ≤18%, and a relative bias ≥-8%. An intercomparison with other available global BA products (GABAM, FireCCI51, C3SBA11, or MCD64) demonstrated that our product (i) exhibits temporal consistency, (ii) represents a significant accuracy improvement, as it reduces BA underestimations by about eightfold, (iii) yields BA estimates four times higher, and (iv) shows enhanced capability in detecting fires of all sizes. The observed BA spatial patterns were heterogeneous across the island, with 32% of

the grasslands burning annually, in contrast to other land cover types such as the dense tropical forest where less than 2% burned every year. We conclude that the BA characterization in Madagascar must be addressed using imagery at spatial resolution higher than MODIS or Sentinel-3 (≥250 m), and temporal resolution higher than Landsat (16 days) to deal with cloudiness, the rapid attenuation of burn scars signals, and small fire patches.

1 Introduction

Fire is a pervasive disturbance that has shaped the distribution of terrestrial biomes, plant evolution and atmospheric composition for millions of years (Lasslop et al., 2019; Kelly et al., 2020). Nowadays, landscape fires affect a vast extent of Earth's surface, with around 5% of ice-free land burning annually (van der Werf et al., 2017; Chen et al., 2023; Fernández-García & Alonso-González, 2023). Despite being a natural and ancient force, contemporary landscape fires are increasingly driven by human activity, and thus are a major element contributing to our rapidly changing world, reshaping fire-prone ecosystems, as well as those that have historically been less prone to fire (Kelly et al., 2020). This context of change poses a global challenge for understanding how fire might affect numerous spheres of global interest. Notably, landscape fires are intricately linked to several of the United Nations Sustainable Development Goals (SDGs), such as Life on Land, Climate Action, Good Health and Well-being, No Poverty, or Zero Hunger, among others (Martin, 2019). Thus, given the far-reaching implications of fire, it is imperative to have accurate spatio-temporal characterizations of this phenomenon available to a wide range of end users (Pereira, 2019). This need is particularly pronounced in regions where fire regimes are rapidly changing, and where the achievement of the mentioned SDGs is further hindered by socio-economic limitations, as it is the case of many regions in tropical Africa (Andela et al., 2017; Fernández-García & Alonso-González, 2023; Omisore, 2018).

In tropical Africa, the island nation of Madagascar stands for its unique biodiversity, with more than 90% of its species found nowhere else (Antonelli et al., 2022; Goodman, 2022a). At the same time, it ranks among the most burned places on Earth (Andela et al., 2017; van der Werf et al., 2017; Fernández-García and Alonso-González, 2023), with recent studies estimating an annual burned area (BA) between 121,000 and 147,000 km^2, corresponding to 21-25% of the island's land (Fernández-García & Kull, 2023). In Madagascar, fire serves multiple overlapping and sometimes competing interests across a diversity

of landscapes and vegetation types. While many locals use fire for pasture management, crop field preparation or pest and wildfire control, some policy makers and conservationists criticise fires for contributing to deforestation, soil erosion and risks to private properties (Kull, 2002; Kull, 2004). As a result, governments have periodically tried to eradicate or minimise landscape burning, but these efforts have been met with resistance from rural populations who rely on fire for their livelihoods (Kull, 2004). In addition, the scientific community identifies anthropogenic fire as a major factor in Madagascar's landscape transformation and biodiversity loss, particularly within forested areas. However, most tree loss occurs in the absence of large-scale fires (Phelps et al., 2022) urging the development of new fire products for the investigation on the role of small-scale fires (Ralimanana et al., 2022). There is also controversy regarding the open biomes - notably grasslands - that dominate the island and are the main location of fires. Some authors have characterised them as degraded ecosystems (Burns et al., 2016), while others view them as ancient representatives of the island's biodiversity, asserting that fire is an integral part of them (Bond et al., 2008; Solofondranohatra et al., 2020). Apart from this, fire has been identified as a suitable management tool in the open biomes, as well as in the immediate vicinity of forest areas where fire-associated risks can be mitigated by specific fire regimes (Bloesch, 1999; Kull, 2004; Ralimanana et al., 2022).

Despite the interest in understanding and addressing the challenges posed by fires in Madagascar, recent advances in remote sensing and modelling have revealed that the BA in this island has been poorly characterised over time (Fernández-García and Kull, 2023). In Madagascar, as in many regions worldwide, the assessment of BA has traditionally relied on coarse resolution sensors (Andela et al., 2017; Frappier-Brinton and Lehmann, 2022; Phelps et al., 2022; Ralimanana et al., 2022). Among these, the Moderate Resolution Imaging Spectroradiometer (MODIS) instrument stands out as one of the most extensively used sensors, being the basis for the North American Space Agency (NASA) standard BA product MCD64A1 (Giglio et al., 2018), as well as the FireCCI51 from the European Space Agency (ESA) (Lizundia-Loiola et al., 2020), with spatial resolutions of 500 m and 250 m, respectively. Other operational BA products include the C3SBA11 (Lizundia-Loiola et al., 2021), with a spatial resolution of 300 m, produced under the Copernicus Climate Change Service of the European Commission and based on the Ocean and Land Colour Instrument (OLCI) on board Sentinel-3. GABAM (Long et al., 2019), another global BA product, which is based on Landsat imagery at higher spatial resolution (30 m) but with lower temporal resolution (16 days

when using one sensor), provides similar BA estimates than FireCCI50 (Long et al., 2019). Despite this reassuring consistency in BA estimates of the aforementioned databases, validation exercises (Padilla et al., 2014; 2015; Boschetti et al., 2019; Franquesa et al., 2022a; 2022b), along with the start of the Sentinel-2 mission in 2015 (which offers spatial resolution of 20 m for most bands, and a temporal resolution of 5 days when combining its two twin sensors, both resolutions higher than Landsat), have provided groundbreaking estimates that highlight the limitations of all previously mentioned products. In this sense, Roteta et al. (2019) developed the FireCCISFD11 database for sub-Saharan Africa in 2016, which revealed that the BA was 80% higher than previously reported by the MCD64A1. This was mainly due to small fires (<100 ha) which were rarely detected by MODIS (comprising only 5% of the MODIS BA) but contributed to 41% of the BA in FireCCISFD11. Similar results were found by Chuvieco et al. (2022), who developed a second version of this product, FireCCISFD20 for the year 2019. In the case of Madagascar, previous analysis made by Fernández-García and Kull (2023) indicates that the BA estimates from Sentinel-2 in 2016 are around four times higher than those from MODIS and BA estimations from refined BA data showed similar differences for 2000, 2005, 2010 and 2020. Notwithstanding the urgency of transitioning towards the use of higher-resolution sensors for a more accurate characterization of BA, no Sentinel-2 or finer BA product currently exists for Madagascar, other than those for the years 2016 and 2019.

The variety and differences in performance among BA products indicate that BA retrieval is not a trivial task. Firstly, BA detection must cope with the uniqueness of each site in terms of spectral signature, as well as with a wide variety of burning conditions (Chuvieco et al., 2019). To deal with these challenges, most products are based on temporal comparisons of reflectance values, some of which include thermal anomalies at coarse resolution (van der Werf et al., 2017; Giglio et al., 2018; Chuvieco et al., 2018; Lizundia-Loiola et al., 2020). When using Sentinel-2 imagery, the same approach has been used (Roteta et al., 2019), although some researchers have recommended excluding data from coarse resolution sensors and focusing solely on the higher-resolution data provided by Sentinel-2 MultiSpectral Instrument (MSI) (Roy et al., 2019). One approach entirely based on finer imagery is the use of supervised multitemporal image analysis. This approach has been used, for example, to obtain BA reference data for validation purposes (Boschetti et al., 2019; Roteta et al., 2021a; Franquesa et al., 2020). Among these methods, a novel option is the use of two-phase algorithms. In the first step, these algorithms create a seed region

composed of pixels with a high probability of being burned. The second phase consists of expanding the seed region by incorporating neighbouring pixels that meet certain criteria, such as having similar spectral characteristics and being spatially connected to the seed region (Bastarrika et al., 2014; Roy et al., 2019; Lizundia-Loiola et al., 2020; Roteta et al. 2021a; Sali et al., 2021). Two-phase algorithms can be effective at detecting complex burned patterns, such as those found in Madagascar, and they are expected to provide more accurate results than simple pixel-based classifications by reducing commission errors due to the use of seeds (Roteta et al. 2021a).

Once a BA product is developed, it is critical to assess its accuracy to inform end-users about the data quality (Boschetti et al., 2009; Chuvieco et al., 2019; Franquesa et al., 2022a). This process, known as validation, can be challenging and time-consuming due to the scarcity of available reference data of higher reliability than the products being validated (Roy et al., 2008; Franquesa et al., 2020). Validation typically involves a spatial comparison of the BA products with the reference BA, a process often referred to as spatial validation. On the other hand, the product's ability to accurately detect the time of burning, is also relevant for some applications and its assessment is referred to as temporal validation. Both spatial and temporal validation assess different errors, but temporal errors often affect the estimates of the spatial assessments, a fact that can be limited with the use of long temporal reference units (Franquesa et al., 2022b). When validating Sentinel-2 products, acquiring long temporal reference units at higher spatial resolution than the product to be validated is currently infeasible using non-commercial satellite imagery (Chuvieco et al., 2019), so previous studies have generated independent and higher-quality reference BA data by comparing subsequent pairs of Sentinel-2 images and employing expert human-based image interpretation (Roteta et al., 2019).

In this work, we present a new BA database for Madagascar covering the period 2016-2022 based on Sentinel-2 imagery (MGBAS2). Specifically, (i) we described how the database was built; (ii) we performed a spatial validation of the product using a pioneering approach of long temporal reference units; (iii) we performed a temporal validation of the product by comparing it with the VIIRS hotspots; (iv) we compared our database with other available BA products to show its interannual

consistency, as well as its outperformance over Landsat, Sentinel-3 and MODIS derived BA data; and (v) we provide new insights on Madagascar's BA based on the presented database.

2 Materials and methods

The methods section in this work comprises five different blocks (Fig. 1). First, we explained how the MGBAS2 product was built with a procedure based on BAMT v1.7 (Roteta et al., 2021a). Second, we performed a spatial validation with new independent long-temporal reference units as recommended by Franquesa et al. (2022b) and analogous methods to those used to validate similar products (Chuvieco et al., 2022). These reference units were made publicly available in the validation burned area (BA) database BARD (https://doi.org/10.21950/YYZNNN; Franquesa et al., 2023). Third, we accomplished a temporal validation based on VIIRS hotspots to identify the timing error in BA detection. Fourth, we compared the BA and accuracy of MGBAS2 with other available BA data from several satellites. Lastly, we computed some direct outputs from our product, including fire frequency, seasonality, and mean annual fraction of burned land by ecoregions and land cover classes.

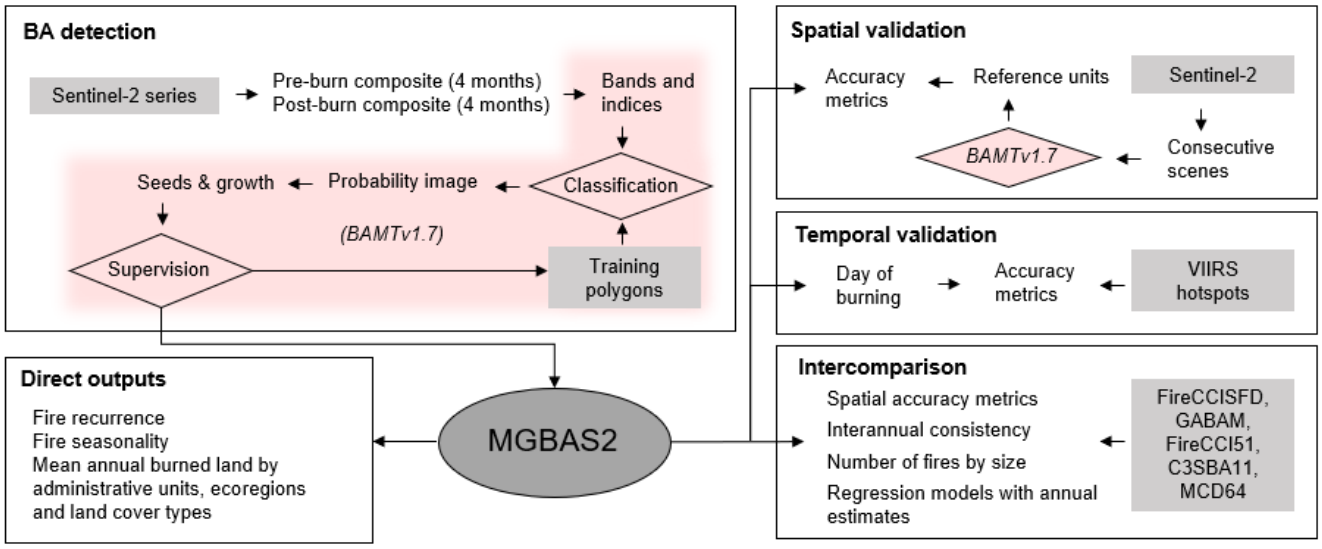

Figure 1: Methodology overview.

2.1. Building the MG-BAS2 database

The BA was identified following a change detection approach, one of the most utilised for BA detection (Chuvieco et al., 2019; Liu et al., 2020; Gaveau et al., 2021). This approach is based on comparisons between the pre- and post-burn reflectance values. A total of 75,010 Harmonized Sentinel-2 1C scenes, spanning from 31 August 2015 to 31 December 2022, were used to build temporal composites with six reflectance bands: blue (B2), green (B3), red (B4), near infrared (B8A), and the two short wavelength infrareds (B11, B12). These were subsequently compared by pairs, each pair representing pre- and post-burn conditions. Sentinel-2 scenes comprised the 2A sensor for the entire study period along with the 2B sensor since March 2017. The Level-1C (top of atmosphere reflectance; Sentinel-2 MSI User Guide, 2023) was preferred over the Level-2A for temporal consistency, and to avoid the already reported noise included by the Sen2Cor correction in the Level-2A scenes (Roteta et al., 2021a). The composites were built for periods of four months by selecting land quality observations with the most prominent signals of BA. Specifically, we created a mask to omit clouds, cloud shadows and bright surfaces. We did this based on bitwise operations, first masking bits 10 (cloud) and 11 (cloud shadows) of the QA60 band, as well as pixels with values greater than 1500 in the B1 band. From these quality observations, we captured the lowest Normalized Burn Ratio Index (NBR) values, which ensures maintaining burned signals. Four-month periods (breakpoints on 30 April, 31 August, and 31 December) were selected to maximise the probabilities of getting cloud-free images while keeping a low probability of repeated burning in subsequent composites.

Once the composites were built, a minimum of 10 training burned and unburned polygons (>40 ha each) were randomly distributed, with at least two polygons per major land cover type (forest, grassland, cropland, sparse vegetation/bare soil, and water bodies). The allocation of the mentioned training polygons and distribution was ensured in the proper locations by visual inspection of RGB false colour composites (Sentinel-2 bands B12, B8A, B4) from the first (pre-fire) and second (post-fire) temporal composites and their difference. The training polygons were used to train the BAMT v1.7 random forest algorithm (Roteta et al., 2021a). This algorithm uses the six spectral bands (B2, B3, B4, B8A, B11 and B12) and three indices: the Normalized Difference Vegetation Index (NDVI), the NBR, and the Enhanced Normalized Burn Ratio (NBR2). These indices were computed for both the post-fire composite and for the difference between the pre- and post-fire composites. The spectral

bands, combined with these spectral indices, served as the input for the random forest algorithm. This process resulted in a BA probability map that allows the identification of seed pixels (i.e., pixels with a high probability of being burned). The seeds and probability images resulting from each image-composite pair comparison were visually inspected in the Google Earth Engine platform, typically zooming in to a scale of 1:20,000. The visual inspection involved comparing the mapping results (seeds and probability images) with burned patches identified by two expert interpreters. The comparison was based on RGB false-color composites (B12, B8A, B4) of the two scenes. Visual inspections were carried out in a minimum of 10 regions, each covering 60 km². These regions were chosen independently from the training areas (i.e., regions with training polygons were avoided) and were randomly selected across the mapping area (i.e., Madagascar), encompassing the five major land cover types mentioned above. The training process was repeated with further training areas until satisfactory results were obtained, that is, no classification errors were visually detected by the expert interpreters. Then, all those pixels with an equal or greater than 50% probability of being burned, and that were spatially connected to at least one seed, were classified as burned. The date of observation for the pixel in the post-burn composite (minimum NBR in the four-month period) was retained for all the pixels classified as burned. The entire protocol was implemented in Google Earth Engine using as reference the code provided by Roteta et al. (2021a).

2.2. Spatial validation analyses

The reference BA databases (Franquesa et al., 2020) were explored and the scarcity of enough reference BA data for a robust validation of the developed product in Madagascar was confirmed, with no more than a single validation area per year. Consequently, we produced and made publicly available (BARD database, Franquesa et al., 2023) our own independent reference BA dataset for two years in Madagascar (2021 and 2019). The year 2021 was randomly selected, and 2019 was selected for convenience due to the availability of several BA products used in this study for intercomparisons. The validation procedure followed the recommended 'good practices' for land cover validation procedures, which involves several steps: implementing a probability-based sampling design, formulating a response design that encompasses the generation of reference data, and conducting the analysis to derive the accuracy metrics (Olofsson et al., 2014). In relation to the reference data,

Olofsson et al. (2014), state that if the validation is conducted using the same source material, the development of reference data of higher quality than the map classification can be achieved by using more accurate classification methods than those used in the map. Likewise, we have considered recent advances on BA validation (Chuvieco et al., 2022; Franquesa et al., 2022b) that show the need of using randomization (Olofsson et al., 2014) as well as long temporal reference units to reduce the impacts of dating errors (Franquesa et al., 2022b). Moreover, we found the most suitable approach to be the computation of BA for each comparison between consecutive pairs of Sentinel-2 scenes, repeating the process over the longest possible period. This method offers higher quality data at 20 m spatial resolution than the one reported by our product based on four-months mosaics and thus is appropriate for validation (Roteta et al., 2021a; Chuvieco et al., 2022; Franquesa et al., 2022b). Accordingly, our validation protocol involved the following steps:

- Spatial definition and selection of reference units: the sampling units for validation purposes were spatially defined based on the tessellation of Sentinel-2 MSI images. All the Sentinel-2 tiles covering the island of Madagascar were selected, a total of 95. To increase the total population of sampling units and facilitate the reference BA retrieval task, each tile was divided into four smaller units of approximately 50 x 50 km. To each tile subdivision, we added a sequential numeric index to the tile identifier (e.g., 38JMT_1). Then, following Stroppiana et al. (2022), all sampling units located in different Sentinel-2 orbits and UTM zones were discarded, obtaining a total population of 242 sampling units (Fig. 2). We applied a stratified random sampling with one level of stratification based on the amount of fraction of land burned in each sampling unit, according to our MGBAS2 product. First, we compute the percentage of burned land in each sampling unit, and then units were stratified into two strata (low and high proportion of burned land) based on a threshold set in the 80th percentile of the BA proportion of the total population. Then, we randomly selected a total of four and two sample units in the low and high stratum, respectively. This sampling was performed for the randomly selected year 2021 and the same sample units were used for the year 2019. The selected sample units were the 38JMT_4 (0.47% of burned land according to MGBAS2 for 2021), 38KQA_132 (4.1%), 38KMC_38 (9.8%), and 38KMG_54 (30.4%) for the low proportion of burned land stratum, and 38KPV_127 (39.5%) and 38KPE_111 (66.7%) for the high proportion of burned land stratum (Fig. 2).

- Temporal definition of reference units: for the definition of the temporal length of our reference BA units we followed the criteria of reaching a compromise between the minimization of the temporal difference between the acquisition dates of pairs of images and the maximisation of the temporal length of the unit (temporal extent of the set of multiple scenes used for pair comparisons) (Franquesa et al., 2022b). Both criteria are highly relevant, but one might constrain the other. On the one hand, spectral signals that enable the identification of BA from satellite platforms might disappear quickly, particularly in grassy and savannah biomes and under wet and productive conditions (Melchiorre and Boschetti, 2018). On the other hand, the length of the validation unit is essential for spatial validations in order to mitigate the impact of temporal errors on spatial accuracy metrics. To optimise both criteria we first identified all Sentinel-2 MSI scenes with a cloud clover less than 15% for the whole year (2019 and 2021), and then we identified pairs of consecutive images with a temporal maximum difference of 16 days. When the difference between consecutive pairs was longer than 16 days, the image composites (B12, B8A, B4) and their NBR differences were visually inspected to guarantee that all the potential fire scars were easily identifiable, using as reference the visual evidence of former scars in the newest scene. When there was not a clear persistence of the BA signal, the selection procedure was re-started from this date onwards. We set the minimum length of the reference units to 40 days. The long temporal reference units obtained ranged between 40 and 209 days for 2019 and between 40 and 225 days for 2021.

- Computation of long temporal reference BA data: the reference BA data was computed from the spatially and temporally defined reference units by applying the protocol described by Roteta et al. (2021a) and similar to the validation of the ESA FireCCISFD20 product (Chuvieco et al., 2022). This is providing training polygons, applying the BAMT v1.7 random forest algorithm, supervising the resulting classification and finally generating a BA layer for each consecutive Sentinel-2 image pair. Then, all the resulting perimeters were combined to generate an ESRI© shapefile with the reference BA data for each of the reference units.

- Accuracy analysis: we calculated a confusion matrix for each of the six reference units from the areas of agreement and disagreement obtained by crossing the reference BA data with our BA product. Then, we calculated the Dice coefficient, omission error, commission error, and relative bias (formulas available in Padilla et al., 2015 and Franquesa et al., 2022b). The unobserved regions in the BA product were considered as unburned areas when computing the accuracy statistics, whereas the unobserved areas in the reference BA data were excluded from the analysis. Global accuracy estimates were inferred for the assessed years (2019 and 2021) using a stratified ratio estimator (Cochran, 1977).

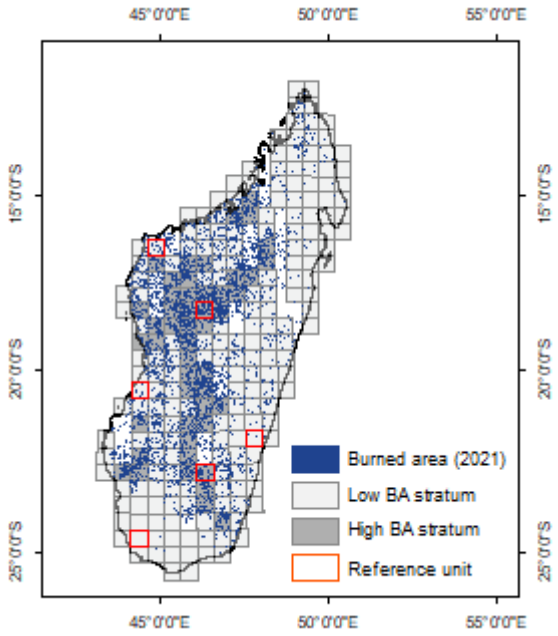

Figure 2: Total population of sampling units defined for validation purposes by strata (low and high fraction of burned land), and location of the six reference units selected for the spatial validation.

2.3. Temporal validation analyses

The temporal reporting accuracy was assessed by conducting a comparative analysis of the product with the dates of VIIRS hotspots (VNP14IMGML) between 2016 and 2021, using a methodology consistent with previous research (Boschetti et al., 2010; Giglio et al., 2018; Lizundia-Loiola et al., 2020; Roteta et al., 2019; Roteta et al., 2021b; Chuvieco et al., 2022).

Specifically, we compared each VIIRS hotspot date with the date of burning in the MGBAS2 product in the same location, and we calculated the percentage of cases in which both products matched with differences <1, <5, <10, <15, <20 and <50 days.

2.4. Intercomparison with other products

We have conducted intercomparisons of MGBAS2 with other products to complement our spatial validation and demonstrate the temporal consistency of our product as well as to showcase the advancements it represents over the existing data. The intercomparisons were made with the FireCCISFD (FireCCISFD11 and FireCCISFD20), GABAM, ESACCI51, C3S11 and MCD64 which represent BA from different satellite platforms, sensors, and resolutions.

- FireCCISFD is the Small Fire Database product from the European Space Agency (ESA) Climate Change Initiative (CCI). The FireCCISFD is available for Sub-Saharan Africa for the years 2016 (FireCCISFD11; Roteta et al., 2019) and 2019 (FireCCISFD20; Chuvieco et al., 2022). FireCCISFD11 and FireCCISFD20 are primarily based on Sentinel-2 MSI sensors at 20 m spatial resolution. The algorithms used to build FireCCISFD11 and FireCCISFD20 are the same but the first uses MODIS active fires (1000 m spatial resolution) and Sentinel-2A imagery, whereas FireCCISFD20 uses VIIRS active fires (375 m spatial resolution) and both A and B Sentinel-2 imagery (Chuvieco et al., 2022).

- GABAM (Long et al., 2019) is a global product based on all the Landsat images available on GEE platform for the period 1984-2020 with a spatial resolution of 0.00025 degree (approximately 30 m). The revisit period for each Landsat platform is 16 days, but the years when more than one platform is available, the combined revisit period decreases. In this work we used the only available version (GABAM V1) (Long et al., 2021).

- FireCCI51 (Lizundia-Loiola et al., 2020) has been developed in the framework of the Climate Change Initiative (CCI) and is the reference global BA product from the European Space Agency (ESA) until 2020. It is based on MODIS imagery incorporating some of bands at 250 m, conferring that final spatial resolution to the product.

- C3SBA11 (Lizundia-Loiola et al., 2021) offers continuity to the FireCCI51 product since 2017 adapting the BA detection procedures to the Sentinel-3 OLCI on board of the twin satellites (A and B). Sentinel-3 OLCI presents similar spatial and temporal resolution than MODIS, with a 300 m pixel size and a revisit of <2 days when Sentinel-3 A and B platforms are combined.

- MCD64 (Giglio et al., 2018) is the NASA standard BA product, which has been produced since 2001 from MODIS imagery at 500 m spatial resolution. MODIS instruments are on board two satellite platforms (Terra and Aqua) resulting in a combined revisit period of around 1 day. In this work we used the pixel version MCD64A1 (collection 6.1) and the gridded product MCD64CMQ.

The FireCCISFD, GABAM, FireCCI51, C3SBA11 and MCD64 were compared with MGBAS2 in different ways. First, we calculated the spatial accuracy metrics as described in Section 2.2, performing spatial validation analyses for the formerly existing products using the six selected reference units and validation periods in 2019 and 2021. The use of same reference sites and periods for validating a set of BA products minimise differences due to sampling so the accuracy metrics are totally comparable. The GABAM product was excluded from this analysis as it does not provide dates of burning. Second, we studied the temporal evolution of the land burned in Madagascar since 2016 normalising the BA in the products to the BA detected in the MGBAS2 (i.e., MGBAS2 BA was set to 100%). Third, for the year 2019, the only one where all the products were available, we performed a comparison of the number of fires (i.e., patches with different burning dates) by fire size class. The selected fire size classes were <0.25 km^2, 0.25 to <1.25 km^2, 1.25 km^2 to <2.5 km^2, and ≥2.25 km^2 as in the analysis of the FireCCISFD20 database (Chuvieco et al., 2022). Also, for 2019 we aggregated the area burned in each product at 0.25-degree (or we acquired the gridded products when available), and then we computed univariate linear regression models with each of

the former products (independent variable) and MGBA2S2 (dependent variable), showing the R^2, bias and root mean square error (RMSE) statistics. All the BA and fire size calculations were made in the sinusoidal equal area projection.

The FireCCISFD pixel products (product names FireCCISFD11 and FireCCISFD20) were acquired from the ESA CCI Open data portal (https://climate.esa.int/en/odp/), the GABAM product was acquired from the Harvard Dataverse available at https://doi.org/10.7910/DVN/3CTMKP, FireCCI51 and C3SBA11 pixel and gridded products were acquired from Copernicus Climate Data Store (https://cds.climate.copernicus.eu/). The MCD64 product was acquired at the pixel level (product name MCD64A1) from the NASA Earth Data Server (https://www.earthdata.nasa.gov/) and the gridded version (product name MCD64CMQ) for intercomparisons from the University of Maryland server (sftp://fuoco.geog.umd.edu). The same server from the University of Maryland was used to download VIIRS active fires (product name VNP14IMGML).

2.5. Calculation of direct outputs

The MGBAS2 product was used to calculate some direct outputs for the whole of Madagascar. For instance, we calculated the number of times that each pixel burned between 2016 and 2022. In addition, we calculated the proportion of burns occurring within the fire season at the pixel level between 2016 and 2022. To do this, we defined the fire season for Madagascar as those months with a mean Fire Weather Index (FWI) higher than 17 (from June to November, inclusive), which has been used as a threshold to define high fire risk (Fernandes, 2019). The FWI mean monthly values were extracted from the Merra2 IMERG.FINAL.v6 available at the NASA Center for Climate Simulation (NCCS) for the period 2001–2019. We also calculated the proportion of burned land within each *commune* (a Malagasy administrative level) for the period 2016–2022, the proportion of burned land by ecoregions (Olson et al., 2001) between 2016 and 2022, and by land cover type after 2019 as we used the GLAD land cover map of 2019 (Hansen et al., 2022) to identify the land cover classes.

3 Results

3.1. Product presentation

The MGBAS2 product covers the period from 1 January 2016 to 31 December 2022, and is distributed in an ESRI© shapefile format for periods of four months. Each shapefile covers the whole of Madagascar. The attribute field named "BurnDate" includes the date of burning in a Year-Month-Day format (YYYYMMDD) (Fig. 3). This field might have zero values, indicating areas that were masked due to the lack of land quality observations. The area without any information in the shapefile was identified as unburned. The spatial resolution corresponds to a 20 m pixel size. A visual example of the MGBAS2 product is shown in Fig. 3.

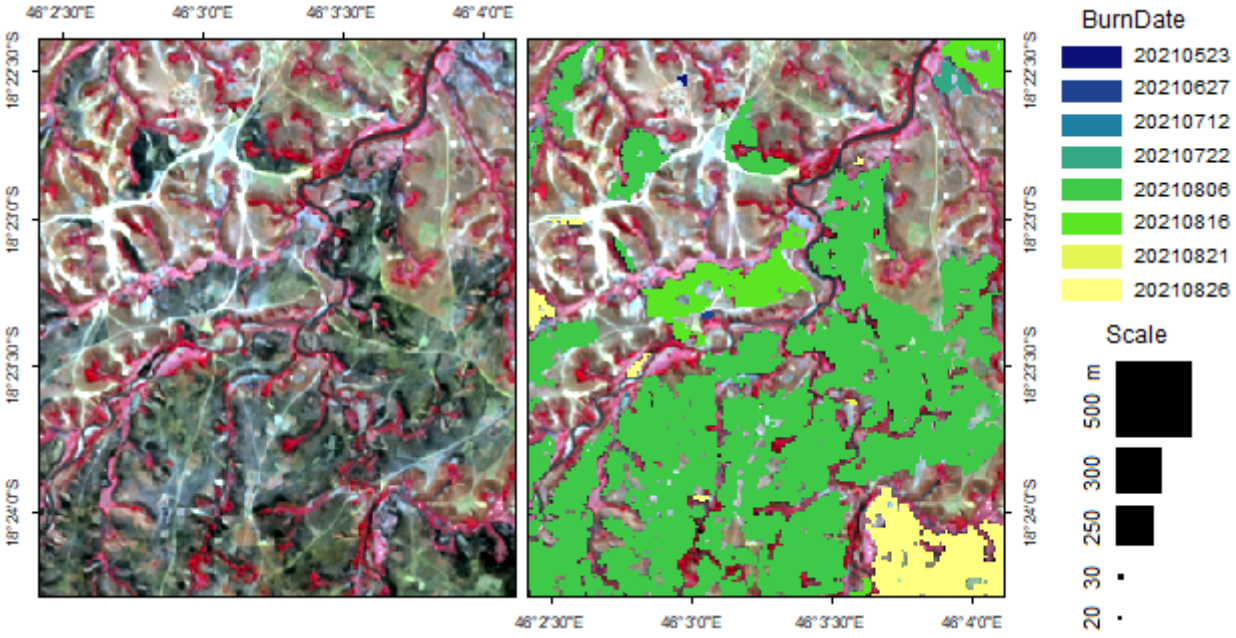

Figure 3: Left panel: example of a Sentinel-2 false colour composite (RGB: B8, B4, B3) acquired on 26 August 2021, with burned areas represented in black and grey tones; right panel: MGBAS2 product between 1 May and 26 August 2021 coloured by the date of sensing of burned area in the panel on the right on the same Sentinel-2 false colour composite. The scale is represented as pixel sizes, including the pixel size of the MGBAS2 product (20 m) and of other BA products (FireCCISFD 20 m, GABAM 30 m, FireCCI51 250 m, C3SBA11 300 m and MCD64A1 500 m).

3.2. Spatial validation

The spatial validation of our product showed Dice coefficients of 78.85% and 83.61% for the years 2019 and 2021, respectively, where 0% indicates no overlap and 100% indicates total similarity between MGBAS2 and the reference data. The results also showed burned area (BA) underestimations of around 8% for both years, omission errors of 24.26% for 2019 and 19.81% for 2021, and smaller commission errors of 17.77% and 12.63% for 2019 and 2021, respectively (Table 1).

Table 1: Global accuracy metrics (± standard error) of the spatial validation of MGBAS2, FireCCISFD20, FireCCI51, C3SBA11 and MCD64A1 products for Madagascar.

BA product	Year	Dice coefficient (%)	Relative bias (%)	Omission error (%)	Commission error (%)
MGBAS2	2019	78.85 ± 4.82	-7.89 ± 4.41	24.26 ± 7.89	17.77 ± 5.09
	2021	83.61 ± 3.86	-8.20 ± 6.97	19.81 ± 6.57	12.65 ± 1.04
FireCCISFD20	2019	84.12 ± 1.48	-0.90 ± 2.79	16.27 ± 2.51	15.48 ± 0.91
FireCCI51	2019	36.66 ± 4.39	-64.47 ± 4.17	75.16 ± 3.72	30.08 ± 3.04
C3SBA11	2019	30.19 ± 3.10	-73.77 ± 2.54	80.94 ± 2.54	27.24 ± 2.52
	2021	21.15 ± 8.99	-82.06 ± 7.71	87.53 ± 6.10	30.49 ± 6.70
MCD64A1	2019	32.50 ± 5.18	-71.90 ± 6.04	79.18 ± 4.29	25.93 ± 1.80
	2021	26.18 ± 6.00	-79.52 ± 5.31	83.95 ± 4.34	25.28 ± 2.20

3.3. Temporal validation

Comparing the BA detection dates with VIIRS hotspots we found that MGBAS2 was able to detect 4.59 ± 0.53% of VIIRS hotspots within the same day, and a 51.86 ± 4.19% in less than 20 days difference. If we expand the period of analysis to 50 days, we observe that 82.11 ± 2.80 of the VIIRS hotspots have a corresponding BA in the MGBAS2.

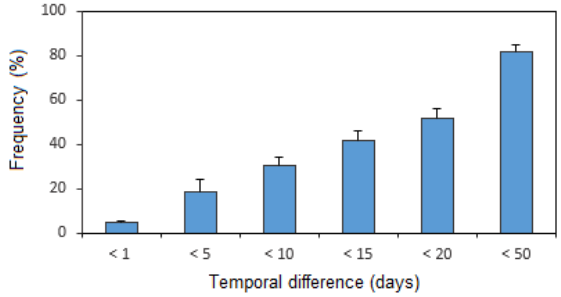

Figure 4: Frequency of VIIRS hotspots detected by MGBAS2 within different time frames.

3.4. Intercomparison

The intercomparison of accuracy metrics among BA products in 2019 and 2021 revealed similar performance among the Sentinel-2-based products (MGBAS2 and FireCCISFD20), which were by far more accurate than the other products based on different sensors (Table 1). The Sentinel-2 products reached Dice coefficients ≥78.85% whereas for the rest were ≤36.66%. The differences in relative biases were also remarkable with the Sentinel-2 based products showing underestimations up to 8.20% and the other products detecting at least 64.47% less BA than the reference data (i.e., MGBAS2 reduced BA underestimations by about eightfold). The omission errors of Sentinel-2 based products were around four times less than the rest, and the commission errors were approximately the half. Results also showed some differences among the coarse-resolution products (FireCCI51, C3SBA11 and MCD64A1), the FireCCI51 being the most accurate.

The accuracy analysis for the years 2019 and 2021 (with long temporal reference units) was supplemented with an analysis of the annual BA detected by each product relativized to the BA detected in MGBAS2. This offered an annual comparative overview from 2016 onwards and provided insights on the Landsat-based BA product that was not included in the accuracy analyses because it lacks burning dates. Results showed that the difference in BA estimates between the Sentinel-2 based products and the rest was consistent over time and revealed that GABAM performed similarly to coarse-resolution products in terms of total annual BA for Madagascar. Thus, all the products not based on Sentinel-2 imagery detected at least four times less BA than those based on Sentinel-2 imagery, with the BA in FireCCI51 (the non-Sentinel-2 product exhibiting the best performance) being 23.25% of the value detected in MGBAS2 (Fig. 5A).

Results showed that Sentinel-2 based products not only detected more BA but also a higher number of fires (Fig. 5B). Sentinel-2 based products detected more fires globally and for all the analysed fire size categories, but the main difference was found in the number of fires with small size (<0.25 km^2). Comparing the MGBAS2 with the FireCCISFD20 we found that the FireCCISFD20 detected more small fires (0 to <1.25 km^2) whereas the MGBAS2 detected more large fires (≥2.5 km^2), which can be attributed to the assignation of burned patches close in time to a same date in the compositing procedure, when NBR values did not decay rapidly. Another difference observed between Sentinel-2 products is the large extent of unmapped regions of the FireCCISFD20 for some months, particularly from January to April (Fig. S2), which on the contrary are mapped by MGBAS2.

The correspondence in global estimates between the Sentinel-2 products presented above was made extensive to a spatial correspondence, as the linear models performed for 2019 with the MGBAS2 and FireCCISFD20 estimates of the percentage of burned land at 0.25º showed a close relationship (R^2 = 0.89; bias = 0.03%) (Fig. 5C). In contrast, the relationships with GABAM, FireCCI51, C3SBA11 and MCD64 gridded data for 2019 were weaker ($R^2 \leq 0.51$) and biased (bias ≥ 18.41) in the line with the reported relative biases, commission, and omission errors (Table 1). Results of the regressions for the rest of years are similar to those found for 2019, and available in Fig. S1.

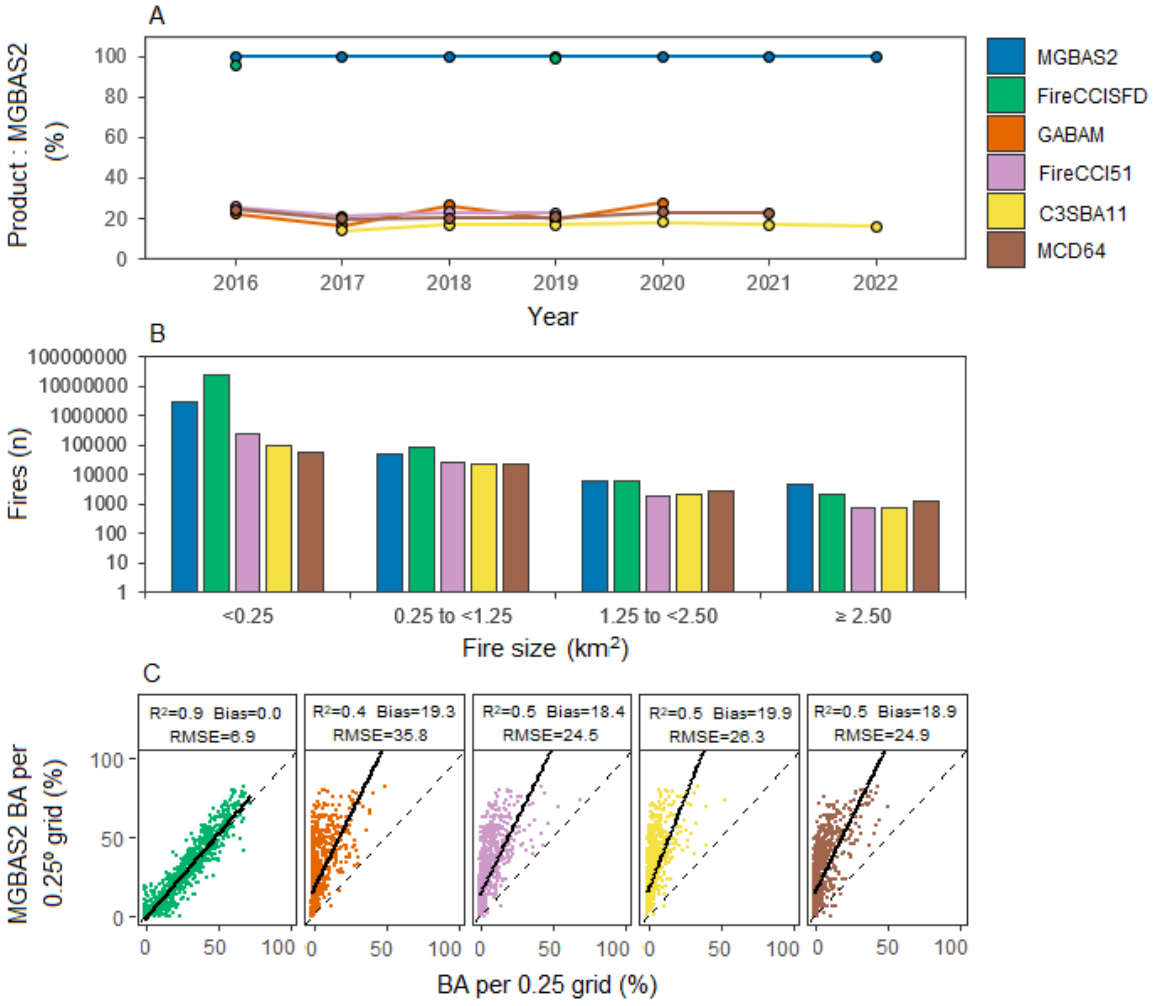

Figure 5: Intercomparison between MGBAS2 and other available BA products. A: temporal evolution of the fraction of annual burned land relativized to the fraction detected by MGBAS2. B: distribution of fires (burned area patches) by fire size classes. C: linear regression models between the fraction of annual burned land detected by MGBAS2 and other available BA products using data aggregated at 0.25º grids.

3.5. Direct outputs

We found that between 20 and 30% of Madagascar's land burns every year, averaging an annual BA of 145,295 km^2 (Table S1). The number of times that the same area burned between 2016 and 2022 ranged from zero to 14 according to MGBAS2, although pixels that burned more than seven times were scarcely represented (<0.40% of Sentinel-2 pixels). Specifically, 43.42% of Sentinel-2 pixels did not burn during the whole period, and a gradual decrease was observed from areas burned

403 once (16.90%) to those burned seven times (3.46%), with the recurrence of fires being inversely proportional to the burned
404 extent (Fig. 6A). The most frequently burned zones were detected in the Central Highlands and western Madagascar where
405 significant proportions of land exhibit annual and biennial burning (Fig. 6A). We also found that most burns in Madagascar
406 are between June and November except for some regions in the eastern coast and in the north where burns outside this period
407 dominate (Fig.6B). The quantification of BA by *commune* showed large differences with values ranging from 5.19 ± 0.09%
408 (mean ± standard deviation) of land burned annually in a *commune* in the region of Analanjirofo (northeast Madagascar) to
409 73.56 ± 3.90% in a *commune* in the region of Bongolava (central Madagascar) (Fig. 6C). The interannual variability also
410 showed a large spatial heterogeneity, with the largest differences in the south, particularly in *communes* in the regions of
411 Ihorombe and the north of Anosy (Fig. 6D). Analysing the percentage of land burned annually by ecoregions (Table 2), the
412 spiny thickets were the least burned at 7.36 ± 2.58%, followed by lowland forests (7.62 ± 2.01%). Mangroves and ericoid
413 thickets exhibited intermediate values of annual burned land. Succulent woodlands (26.41 ± 6.71%), dry deciduous forests
414 (29.37 ± 2.66%) and subhumid forests (33.78 ± 4.44%, mostly corresponding with the grassy biome in the Central Highlands)
415 showed the highest percentage of land burned each year. Focusing on the major GLAD land cover types in Madagascar we
416 found that the less affected classes were the scarcely vegetated areas as well as the dense tree cover class, the last with 1.70 ±
417 0.32% of land burning annually (Table 2). Intermediate BA values (in percentual terms) were observed in the major wetland
418 types, zones where tree cover is rising, and semi-arid vegetation. The areas that exhibited tree cover loss not related to fire
419 between 2000 and 2019 according to the reference land cover types, reached 12.82 ± 1.14% of land burned annually. The
420 MGBAS2 also detected that the extent of burning reached 15.75 ± 1.60% of croplands, 16.48 ± 2.48% of the open tree cover
421 and 31.86 ± 2.47% of the dense short vegetation (grassland) annually.

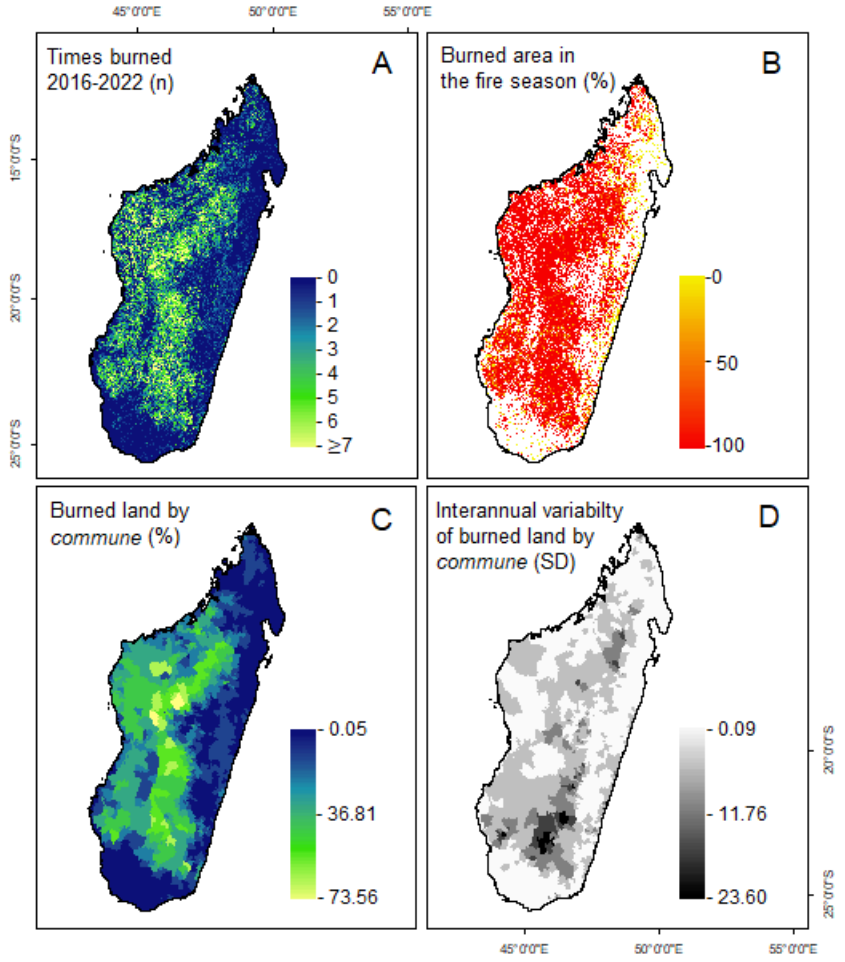

Figure 6: Maps of Madagascar showing the number of times that a same area burned between 2016 and 2022 (A), the proportion of burns within the fire season defined as the period between June and November (B), the proportion of burned land by *commune* (C), the interannual variability of burned land by *commune* (D).

Table. 2: Mean (± standard deviation) burned area by Olson ecoregions (Olson et al., 2001) and by the land cover types defined by Hansen et al., (2022). Note that the values for burned area by ecoregions are 2016-2022 averages, whereas the values by land cover classes are 2020-2022 averages, as the land cover product is based on data up to 2019.

	Burned area	
Ecoregions	% of land	Km^2
Madagascar subhumid forests (Central Highlands)	33.78 ± 4.44	67204.48 ± 8835.32
Madagascar dry deciduous forests	29.37 ± 2.66	44498.09 ± 4033.34
Madagascar succulent woodlands	26.41 ± 6.71	20997.33 ± 5335.42
Madagascar ericoid thickets	14.39 ± 4.85	183.28 ± 61.71
Madagascar mangroves	13.62 ± 2.41	706.65 ± 125.15
Madagascar lowland forests	7.62 ± 2.01	8521.04 ± 2250.08
Madagascar spiny thickets	7.36 ± 2.58	3184.24 ± 1117.13
Land cover classes		
Dense short vegetation	31.86 ± 2.47	91906.09 ± 6550.13
Open tree cover	16.48 ± 2.48	24319.22 ± 2989.51
Cropland	15.73 ± 1.60	2289.87 ± 247.33
Tree cover loss, not fire (2000-2019)	12.82 ± 1.14	4257.98 ± 371.87
Semi-arid	10.76 ± 0.55	3674.26 ± 270.95
Wetland dense short vegetation	10.33 ± 0.45	755.67 ± 55.53
Wetland tree cover loss (2000-2019)	10.14 ± 0.73	73.54 ± 11.45
Built-up	9.63 ± 0.79	261.16 ± 32.97
Tree cover gain (2000-2019)	8.48 ± 1.23	321.89 ± 41.41
Wetland open tree cover	8.36 ± 0.88	698.24 ± 99.35
Wetland tree cover gain (2000-2019)	7.09 ± 1.04	7.52 ± 1.00
Wetland sparse vegetation	3.97 ± 0.88	35.81 ± 18.71
Wetland dense tree cover	1.92 ± 0.30	8.39 ± 2.46
Dense tree cover	1.70 ± 0.32	692.48 ± 150.13
Salt pan	0.33 ± 0.08	0.34 ± 0.19
True desert	0.04 ± 0.01	0.11 ± 0.06

4 Discussion

We have developed a burned area (BA) database for Madagascar (2016–2022) using Sentinel-2 imagery. This is an important advancement in fire science as it is the first BA product based on Sentinel-2 for this island apart from FireCCISFD products that are only available for 2016 and 2019 (Roteta et al., 2019; Chuvieco et al., 2022). In the case of Madagascar, the need of this product was imperative, as using Sentinel-2 imagery we have detected around four times more BA than reported using other satellites. This significant difference should not be omitted when studying fire whether for data records and statistical purposes (Mahood et al., 2022; Andela et al., 2019), analysis of fire impacts (Alonso-González and Fernández-García, 2021; Fernández-García and Alonso-González, 2023) or landscape dynamics potentially driven by fire such as forest loss (Hansen et al., 2022). Likewise, the new estimates provided here might be useful to decrease the currently high uncertainties in the estimates of carbon emissions due to fire (Liu and Yang, 2023).

The validation analyses of our product showed similar accuracy estimates to other Sentinel-2 BA products in tropical regions such as the FireCCISFD developed for Sub-Saharan Africa for two years (Roteta et al., 2019; Chuvieco et al., 2022), or the product developed for Indonesia for 2019 (Gaveau et al., 2021). However, some advantages or strong points of our product should be highlighted when compared with other Sentinel-2 BA products. First of all, our database is the first time series of Sentinel-2-derived BA data over a large region, whereas former products are available for a single year or for two years (Roteta et al., 2019; Gaveau et al., 2021; Chuvieco et al., 2022). Second, the algorithm we used is fully consistent over time, thus facilitating the comparability of seven years of data. This enables not only monitoring over time but also analyses such as the stability of BA values, fire frequency, and the calculation of other fire regime attributes. Third, our database is fully independent from coarse-resolution sources, unlike the FireCCISFD11 and FireCCISFD20, which only map those tiles with hotspots detected by MODIS or VIIRS, respectively and low cloud cover (Roteta et al., 2019; Chuvieco et al., 2022), thus leading to large unmapped regions that might have BA detectable by Sentinel-2 (see Fig. S2, as well as Figs. 1 and 2 in Ramo et al., 2021). It is important to note that this advantage of our product is not reflected in our validation results because of a temporal and spatial reasons. Thus, the generation of long temporal reference units necessitates a focus on the dry season period, thus avoiding January to March, where unmapped areas predominate in the former Sentinel-2 based products. In

addition, the reference units are limited in number and randomly distributed, with scarce representation of areas with absence of MODIS or VIIRS hotspots for the validation period.

Nonetheless, the Sentinel-2 BA products largely outperformed coarse-resolution products, which exhibited higher omission errors for Madagascar than the values reported for global validations (e.g. Padilla et al., 2015; Boschetti et al., 2019; Lizundia-Loiola et al., 2020; Franquesa et al., 2022a; 2022b). The great outperformance of Sentinel-2 products over coarse-resolution products (MODIS- and Sentinel-3-based) can be attributed to the high prevalence of small fire patches which cause the attenuation of BA signals at pixel sizes ≥250 m (Ramo et al., 2021; Franquesa et al., 2022a), as well as to fire shapes, since errors of coarse-resolution products increase as patches are smaller and less compact (Campagnolo et al., 2021; Franquesa et al., 2022a). Both aspects can be particularly relevant in complex landscapes such as those in many parts of Madagascar, where a rough topography predominates with a high density of valleys and ridges, and fine-grained patchy peasant landscapes. There, fires with sizes assumed to be within a single or a few coarse pixels usually extend over numerous pixels where burned and unburned areas mix, magnifying the mixing between burned and unburned spectral signals. This is not only because of the patchy landscape but also because of the burning strategies of Madagascar's inhabitants who burn the landscape in a rotational way over time and space to fit their own interests (Kull, 2004). There are options to address the challenge of getting BA estimates when there are different spectral signals (burned and unburned) within same coarse-resolution pixels, such as applying spectral unmixing methods (Quintano et al., 2005), or statistical approaches that combine the detected BA with other variables such as active fires (van der Werf et al., 2017), landscape fragmentation or social variables to refine BA data (Fernández-García and Kull, 2023). However, the desirable alternative to solve this limitation is the direct use of higher resolution imagery.

In addition to comparing our estimates with the coarse-resolution sensors mentioned above, we have also compared our estimates with those obtained from Landsat imagery. Landsat-derived BA showed underestimations and errors comparable to that from coarse-resolution imagery. Landsat missions started in 1972 and have been used to characterise multiple landscape and land-use change variables for decades. In relation to fire, GABAM is the only available Landsat database at the global

480 scale (the only one covering Madagascar) (Long et al., 2019), although several regional products are available for the
481 Conterminous United States (Hawbaker et al., 2020), Portugal (Neves et al., 2023), or Chile (Miranda et al., 2022) among
482 others, generally showing a high accuracy. However, in tropical regions Landsat's long revisit periods can be a major constraint
483 to proper BA detection, particularly in areas with high cloud cover and rapid fade of burn scars (Chuvieco et al., 2019). This
484 is the case of Madagascar where some regions have a cloud cover leading to a near zero probability of having a Landsat cloud-
485 free observation in certain seasons (Ju and Roy, 2008). In addition, the short persistence of BA spectral signals due to
486 vegetation regrowth is another limitation (Franquesa et al., 2022b). In the grassy biome, which is the dominant land cover in
487 the island, the persistence of BA signals in MODIS imagery has been estimated in between 16 and 48 days, and in the tropical
488 forest the 80.5% of the BA has persistence under 32 days in MODIS imagery (Melchiorre and Boschetti, 2018) that might
489 vary depending on post-burn weather conditions (Franquesa et al., 2022b). Although the limitations of Landsat are very
490 different from those from MODIS or Sentinel-3, we found GABAM estimates similar to those from coarse-resolution sensors
491 in Madagascar.
492
493 The direct analysis of our BA product showed the heterogeneous burning patterns in Madagascar as reported in the literature
494 and previous analyses using remote sensing (Kull, 2004; Andela et al., 2017; Frappier-Brinton and Lehmann, 2022; Phelps et
495 al., 2022), with the highest values of burned land in central Madagascar. We found an insignificant extent showing sub-annual
496 recurrence levels thus indicating the suitability of developing annual presence-absence BA data such as GABAM (Long et al.,
497 2019). Moreover, we found that burns concentrate between June and November, except in the east and in the north where
498 many of the burns were observed out of this period (though one should keep in mind that a detection delay can extend up to
499 50 days). The spatial and temporal patterns of fire relate strongly to farmers and herders' uses of fire. As a rough synthesis,
500 the Central Highlands are dominated by grasslands dotted with cultivated fields, where farmers primarily use fire to meet the
501 needs of livestock as well as an efficient tool for preparing croplands (Kull, 2004; Goodman, 2022b). Focusing on timing,
502 early fires in the grasslands have been associated with pasture renewal (replacement of lignified grasses with new nutritious
503 shoots), woodland protection practices and the control of locust invasions. Pasture fires continue between June and September,
504 while from October, many fires are related to crop field preparation (Kull, 2004). On the contrary, in the eastern lowlands and

in the north, the landscape is dominated by rainforests and agricultural lands. There, fire is more related to shifting cultivation practices (*tavy*), where vegetation is cut and allowed to dry, typically between August and October and soon after burned, before the rainy season (Kull, 2004). Then, the land is cultivated typically between 1-3 years and left in fallow for longer. All these cyclical practices contribute to explain the BA patterns detected in central and eastern Madagascar, with more burned land concentrating in grasslands and croplands, and less in tropical rainforests. In relation to the seasonality, the high proportion of fires after November in the eastern region and in the north is also in agreement with previous work analysing VIIRS hotspots that detected 80% of fires there between October and December (Frappier-Brinton and Lehmann, 2022). The fraction of land that burned annually in the dry deciduous forest and succulent woodland ecoregions (west) was quite high, indeed close to the estimates reached in the open landscapes of the Central Highlands. In the west, pasture maintenance, charcoal production, and expansion of agricultural land play also a major role, with the *tavy* practice in the dry tropical forests traditionally following similar patterns to those in the east, but with earlier burns (Kull, 2004; Scales, 2011; Waeber et al., 2014). In this sense, the analyses of Frappier-Brinton and Lehmann (2022) already highlighted the exceptionally high and increasing number of fires detected by VIIRS hotspots in those two ecoregions, with a 32% of the remaining forests being within 500 m of a fire hotspot in 2016. Our results also found that around 43% of Madagascar's land did not burn between 2016 and 2022. The unburned zones were mostly in the arid south (spiny thickets and southern succulent woodlands), in the northwest, and in urban *communes* as indicated by coarser-resolution analyses (Andela et al., 2017; Frappier-Brinton and Lehmann, 2022; Phelps et al., 2022).

The MGBAS2 has limitations similar to other BA products based on Sentinel-2, which can be related to a still insufficient spatial and temporal resolution and the absence of images before 2015. In relation to the first, it is important to note that many croplands in Madagascar are extremely small, with size even smaller than 20 m × 20 m, which might complicate the detection of some agricultural burns using Sentinel-2. In relation to the temporal resolution, the cloudiness in the east and north led to average periods between cloud-free Sentinel-2 scenes ranging from 18 to 46 days (Sudmanns et al., 2019). In these regions, it is probable that many *tavy* burns are missed, as crops are planted soon after burnings (Kull, 2004). Another limitation of remote sensing BA products is the difficulty of detecting BA below a forest canopy (surface forest fires) because of the shielding

effect of vegetation (van der Werf et al., 2017; Fernández-García et al., 2018). These three limitations affect MGBAS2 as well as the validation data, so fire underestimations might be larger than reported. Computational capacity can also be a limiting factor when producing and working with Sentinel-2 data, a challenge that can be addressed using cloud computing platforms such as Google Earth Engine (Chuvieco et al., 2019). Even with the mentioned limitations, Sentinel-2 provides the most accurate BA estimates among the non-commercial satellites nowadays, and thus we recommend the use of our product for accurate fire monitoring, carbon emission estimation, land use planning, and ecological studies in Madagascar. We also encourage the use of Sentinel-2 BA data for accurate trend analysis in the future. In relation to the last recommendation, we highlight that coarse-resolution underestimations might not be constant over time, as they can be impacted in Africa by an increased number of undetected small fires over time attributed to ongoing increases in landscape fragmentation (Archibald, et al., 2011; Archibald, 2016). This plausible inconsistency of errors over time might be relevant as it can contribute to misleading trend estimates. Future work might attempt to compensate for the historical underestimations from before the Sentinel-2 era by using modelling methods that can take advantage of the new estimates provided here, similarly to Fernández-García and Kull (2023). Likewise, we encourage advancing the field of BA detection by exploring the possibilities that might offer the combination of different multispectral imagery to improve temporal resolution (e.g. Landsat and Sentinel-2; Quintano et al., 2018; Roy et al., 2019), as well as the combination of different sensor types (e.g. by combining multispectral and radar data; Tanase et al., 2015) to reduce the impact of cloudiness on BA detection and timing in the rainforest (Schulte to Bühne and Pettorelli, 2017; Belenguer-Plomer et al., 2021).

Our database represents a significant contribution to several scientific disciplines and to the achievement of the Sustainable Development Goals (SDGs) by providing critical data that support advancements in science, informed decision-making, effective management practices, and ultimately environmental conservation and development. In this sense, concerning the SDG Life on Land, the identification of fire incidence is the initial step in better understanding the actual role of this phenomenon in Madagascar's ecosystems, and in characterizing key fire regime attributes such as fire frequency and seasonality (Bond et al., 2008; Fernández-García et al., 2020; Phelps et al., 2022). These attributes are essential to understand the relationships between fire, habitats and biodiversity, as well as to identify and implement sustainable fire management

555 practices (Ralimanana et al., 2022). Additionally, our database contributes to the SDG Climate Action, by enabling the
556 quantification of carbon emissions from landscape fires with direct observations instead of the currently used models (Chen et
557 al., 2023). Accurate BA mapping also facilitates the estimation of pyrogenic carbon forms, which can act as a carbon sink
558 (Jones et al., 2019; Bowring et al., 2022). Our database further supports advancement in the SDG Good Health and Well-
559 being, as fire smoke is responsible of about 680,000 premature deaths, half of them in Africa (Roberts & Wooster, 2021), as
560 well as of more than 20% of infant deaths in some regions in Madagascar (Pullabhotla et al., 2023) - surely more if estimations
561 were based using high resolution BA data. Therefore, accurate BA data could contribute to epidemiology and public health,
562 and might be useful in assisting for public authorities in identifying critical periods and regions to implement measures to
563 protect people. A high-resolution database is also essential for further unravelling the extent of fire management practices that
564 support local livelihoods, mainly agricultural and livestock production, which account for a large proportion of the economy
565 in Madagascar and sub-Saharan Africa in general (Kull, 2004; Omisore, 2018). Investigating these intricate relationships would
566 potentially contribute to identify suitable management practices supporting the SDGs No Poverty and Zero Hunger, and their
567 relationships with biodiversity conservation, climate change, health and well-being in the complex landscapes of Madagascar.

568 **4 Conclusions**

569 Here we develop, validate, intercompare, and analyze a burned area (BA) database for Madagascar covering the period 2016-
570 2022 (MGBAS2). The database, built exclusively with imagery from Sentinel-2A and 2B sensors, constitutes the first time
571 series of BA data from Sentinel imagery in Africa over a large region, opening multiple analytical possibilities.
572
573 The spatial validation with long temporal reference units revealed high accuracy for the developed product (Dice coefficients
574 ≥79%, omission errors ≤24%, commission errors ≤18%, and a relative bias ≥-8%). Validations also highlighted the need to
575 use satellite imagery with equal or higher spatial and temporal resolution than Sentinel-2 imagery to avoid significant omission
576 errors in Madagascar. In this regard, MODIS, Sentinel-3, and Landsat BA data resulted in omission errors larger than 75% and
577 produced largely biased estimates (at least -64.47% of BA detected).
578

The analyses of the BA data from MGBAS2 showed that between 20 and 30% of Madagascar's land burns every year, but heterogeneous burning patterns were detected. Most of the BA concentrates in Central and Western Madagascar. These regions correspond mostly to the Central Highlands and the dry deciduous forest ecoregion. Likewise, we found that many areas in these fire-prone regions recurrently burn every few years, mostly between May and November.

Data availability

The MGBAS2 database is publicly available and downloadable at Zenodo (https://doi.org/10.5281/zenodo.8201841; Fernández-García et al., 2023). The reference long units developed and used in the present work are published in BARD (https://doi.org/10.21950/YYZNNN; Franquesa et al., 2023).

Appendix

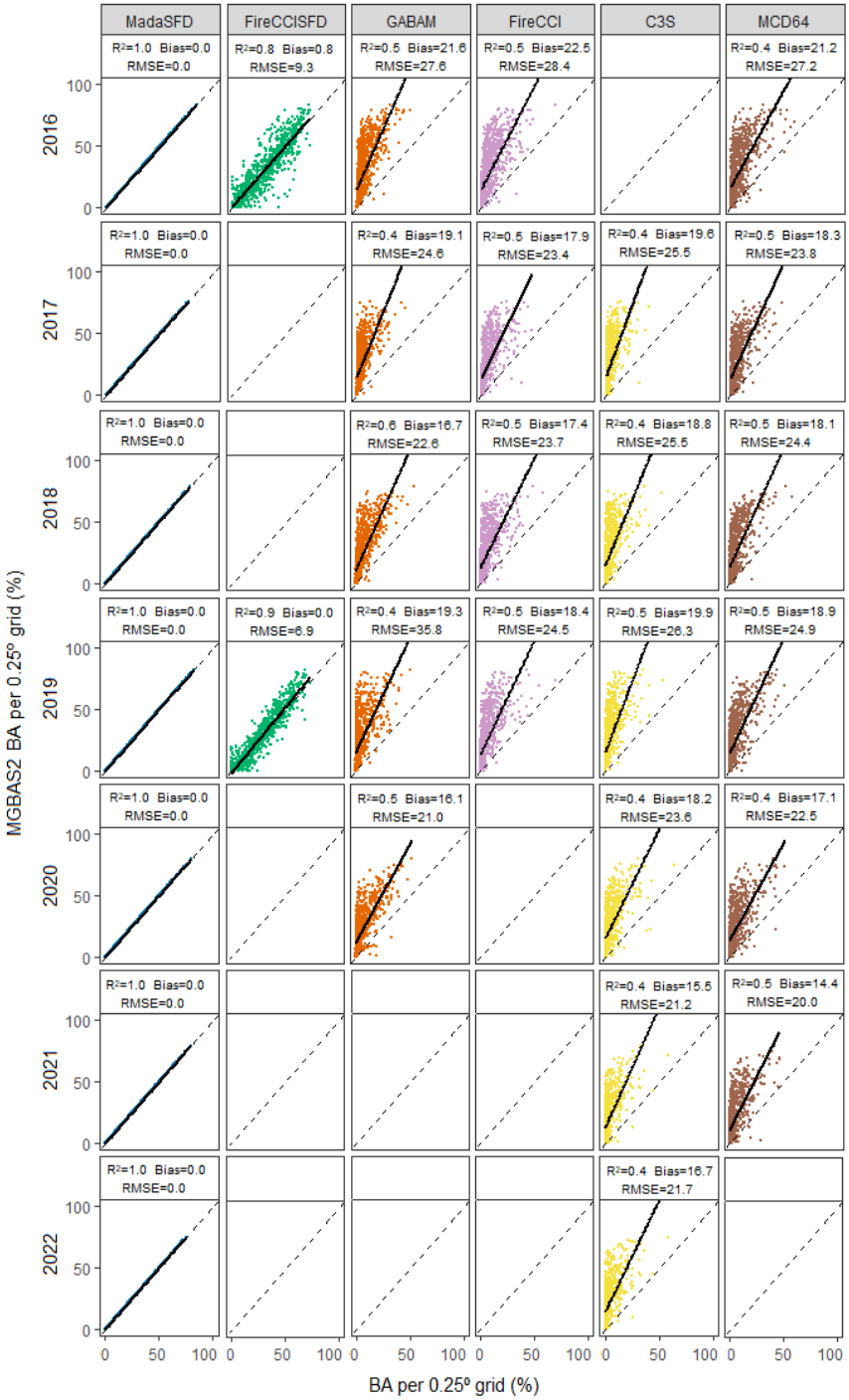

Fig. S1: Regression models between the estimates of the MGBAS2 database and other available burned area products. The analysis was done with the values of burned land aggregated at 0.25-degree cells.

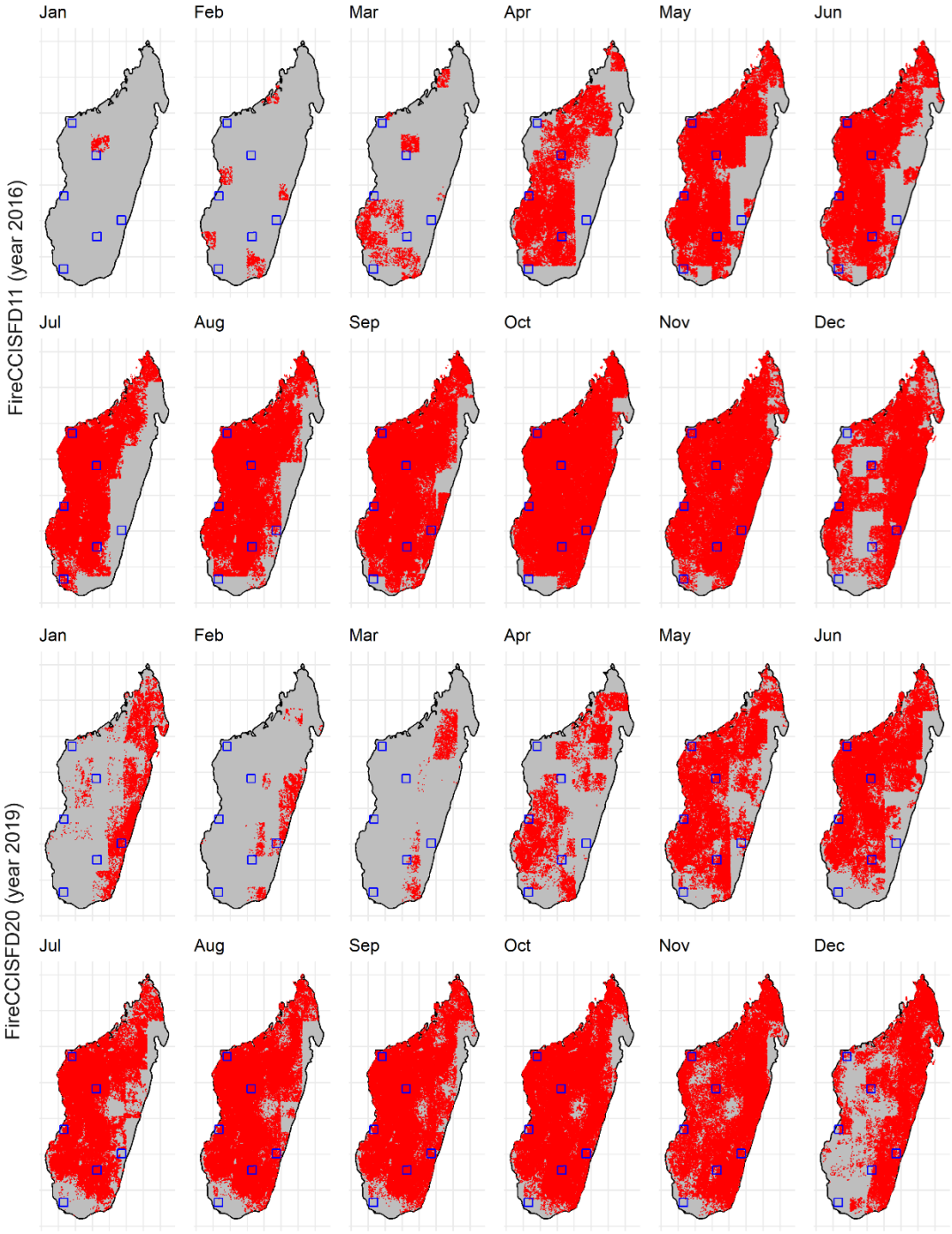

591

592 **Fig. S2: Burned area (BA) by months in the FireCCISFD11 and FireCCISFD20 products in 2016 and 2019 respectively. Borders of**

593 **BA polygons were also coloured in red to highlight the unmapped tiles. Blue squares indicate the location of the reference units.**

Table S1: Burned area detected by MGBAS2 for the period 2016-2022 in Madagascar by years.

Year	Burned area	
	% of land	Km^2
2016	30.23	178833.46
2017	24.72	146209.23
2018	24.72	146196.35
2019	26.12	154510.52
2020	24.33	143930.13
2021	20.45	120980.13
2022	21.37	126406.09

Author contribution

VFG and MF designed the experiments and analyses, VFG built the database and made the intercomparisons with other products, MF and VFG built the long reference units, MF carried out the spatial and the temporal validations, VFG prepared the first draft of the manuscript and MF and CAK contributed to the document, CAK and VFG were responsible for funding acquisition and projects supervision.

Competing interests

The authors declare that they have no conflict of interest.

Acknowledgements

This work has been done with funding from the Swiss Network for International Studies (SNIS) for the project “Fire regimes and ecosystem services in African biodiversity hotspots: can fire policies favoring climate change mitigation, biodiversity and local communities converge?”, and in the framework of the project “Testing the pyrodiversity-biodiversity hypothesis in central Madagascar grasslands” (SR22\100062) granted by the British Ecological Society. VFG is supported by a Margarita

Salas post-doctoral fellowship from the Ministry of Universities of Spain, financed with European Union-NextGenerationEU and Ministerio de Universidades funds and granted by the University of León to conduct his post-doctoral research at the University of Lausanne.

References

Alonso-González, E. and Fernández-García, V.: MOSEV: a global burn severity database from MODIS (2000–2020), Earth Syst. Sci. Data, 13, 1925–1938, https://doi.org/10.5194/essd-13-1925-2021, 2021.

Andela, N., Morton, D. C., Giglio, L., Chen, Y., van der Werf, G. R., Kasibhatla, P. S., DeFries, R. S., Collatz, G. J., Hantson, S., Kloster, S., Bachelet, D., Forrest, M., Lasslop, G., Li, F., Mangeon, S., Melton, J. R., Yue, C., and Randerson, J. T.: A human-driven decline in global burned area, Science, 356, 1356–1362, https://doi.org/10.1126/science.aal4108, 2017.

Andela, N., Morton, D. C., Giglio, L., Paugam, R., Chen, Y., Hantson, S., van der Werf, G. R., and Randerson, J. T.: The Global Fire Atlas of individual fire size, duration, speed and direction, Earth Syst. Sci. Data, 11, 529–552, https://doi.org/10.5194/essd-11-529-2019, 2019.

Antonelli, A., Smith, R. J., Perrigo, A. L., Crottini, A., Hackel, J., Testo, W., Farooq, H., Torres Jiménez, M. F., Andela, N., Andermann, T., Andriamanohera, A. M., Andriambololonera, S., Bachman, S. P., Bacon, C. D., Baker, W. J., Belluardo, F., Birkinshaw, C., Borrell, J. S., Cable, S., Canales, N. A., Carrillo, J. D., Clegg, R., Clubbe, C., Cooke, R. S. C., Damasco, G., Dhanda, S., Edler, D., Faurby, S., de Lima Ferreira, P., Fisher, B. L., Forest, F., Gardiner, L. M., Goodman, S. M., Grace, O. M., Guedes, T. B., Henniges, M. C., Hill, R., Lehmann, C. E. R., Lowry, P. P., II, Marline, L., Matos-Maraví, P., Moat, J., Neves, B., Nogueira, M. G. C., Onstein, R. E., Papadopulos, A. S. T., Perez-Escobar, O. A., Phelps, L. N., Phillipson, P. B., Pironon, S., Przelomska, N. A. S., Rabarimanarivo, M., Rabehevitra, D., Raharimampionona, J., Rajaonah, M. T., Rajaonary, F., Rajaovelona, L. R., Rakotoarinivo, M., Rakotoarisoa, A. A., Rakotoarisoa, S. E., Rakotomalala, H. N., Rakotonasolo, F., Ralaiveloarisoa, B. A., Ramirez-Herranz, M., Randriamamonjy, J. E. N., Randriamboavonjy, T., Randrianasolo, V., Rasolohery, A., Ratsifandrihamanana, A. N., Ravololomanana, N., Razafiniary, V., Razanajatovo, H., Razanatsoa, E., Rivers, M., Sayol, F., Silvestro, D., Vorontsova, M. S., Walker, K., Walker, B. E., Wilkin, P., Williams, J., Ziegler, T., Zizka, A., and Ralimanana, H.: Madagascar's extraordinary biodiversity: Evolution, distribution, and use, Science, 378, https://doi.org/10.1126/science.abf0869, 2022.

Archibald, S.: Managing the human component of fire regimes: lessons from Africa, Phil. Trans. R. Soc. B, 371, 20150346, https://doi.org/10.1098/rstb.2015.0346, 2016.

Archibald, S., Staver, A. C., and Levin, S. A.: Evolution of human-driven fire regimes in Africa, Proc. Natl. Acad. Sci. U.S.A., 109, 847–852, https://doi.org/10.1073/pnas.1118648109, 2011.

Bastarrika, A., Alvarado, M., Artano, K., Martinez, M., Mesanza, A., Torre, L., Ramo, R., and Chuvieco, E.: BAMS: A Tool for Supervised Burned Area Mapping Using Landsat Data, Remote Sens., 6, 12360–12380, https://doi.org/10.3390/rs61212360, 2014.

Belenguer-Plomer, M. A., Tanase, M. A., Chuvieco, E., and Bovolo, F.: CNN-based burned area mapping using radar and optical data, Remote Sens. Environ., 260, 112468, https://doi.org/10.1016/j.rse.2021.112468, 2021.

Bloesch, U.: Fire as a tool in the management of a savanna/dry forest reserve in Madagascar, Appl. Veg. Sci., 2, 117–124, https://doi.org/10.2307/1478888, 1999.

Bond, W. J., Silander Jr, J. A., Ranaivonasy, J., and Ratsirarson, J.: The antiquity of Madagascar's grasslands and the rise of C4grassy biomes, J. Biogeogr., 35, 1743–1758, https://doi.org/10.1111/j.1365-2699.2008.01923.x, 2008.

Boschetti, L., Roy, D. P., Giglio, L., Huang, H., Zubkova, M., and Humber, M. L.: Global validation of the collection 6 MODIS burned area product, Remote Sens. Environ., 235, 111490, https://doi.org/10.1016/j.rse.2019.111490, 2019.

Boschetti, L.; Roy, D.P.; Justice, C.O. International Global Burned Area Satellite Product Validation Protocol Part I-Production and Standardization of Validation Reference Data (to Be Followed by Part II-Accuracy Reporting); Committee on Earth Observation Satellites: Silver Spring, MD, USA, 2009

Boschetti, L., Roy, D. P., Justice, C. O., and Giglio, L.: Global assessment of the temporal reporting accuracy and precision of the MODIS burned area product, Int. J. Wildland Fire, 19, 705, https://doi.org/10.1071/wf09138, 2010.

Bowring, S., Jones, M. W., Ciais, P., Guenet, B., and Abiven, S.: Pyrogenic carbon decomposition critical to resolving fire's role in the Earth system. Nat. Geosci., 15, 135–142. https://doi.org/10.1038/s41561-021-00892-0, 2022

Schulte to Bühne, H. and Pettorelli, N.: Better together: Integrating and fusing multispectral and radar satellite imagery to inform biodiversity monitoring, ecological research and conservation science, edited by: Lecomte, N., Methods Ecol. Evol., 9, 849–865, https://doi.org/10.1111/2041-210x.12942, 2017.

673 Burns, S. J., Godfrey, L. R., Faina, P., McGee, D., Hardt, B., Ranivoharimanana, L., and Randrianasy, J.: Rapid human-induced
674 landscape transformation in Madagascar at the end of the first millennium of the Common Era, Quat. Sci. Rev., 134, 92–99,
675 https://doi.org/10.1016/j.quascirev.2016.01.007, 2016.
676
677 Campagnolo, M. L., Libonati, R., Rodrigues, J. A., and Pereira, J. M. C.: A comprehensive characterization of MODIS daily
678 burned area mapping accuracy across fire sizes in tropical savannas, Remote Sens. Environ., 252, 112115,
679 https://doi.org/10.1016/j.rse.2020.112115, 2021.
680
681 Chuvieco, E., Lizundia-Loiola, J., Pettinari, M. L., Ramo, R., Padilla, M., Tansey, K., Mouillot, F., Laurent, P., Storm, T.,
682 Heil, A., and Plummer, S.: Generation and analysis of a new global burned area product based on MODIS 250 m reflectance
683 bands and thermal anomalies, Earth Syst. Sci. Data, 10, 2015–2031, https://doi.org/10.5194/essd-10-2015-2018, 2018.
684
685 Chuvieco, E., Mouillot, F., van der Werf, G. R., San Miguel, J., Tanase, M., Koutsias, N., García, M., Yebra, M., Padilla, M.,
686 Gitas, I., Heil, A., Hawbaker, T. J., and Giglio, L.: Historical background and current developments for mapping burned area
687 from satellite Earth observation, Remote Sens. Environ., 225, 45–64, https://doi.org/10.1016/j.rse.2019.02.013, 2019.
688
689 Chuvieco, E., Roteta, E., Sali, M., Stroppiana, D., Boettcher, M., Kirches, G., Storm, T., Khairoun, A., Pettinari, M. L.,
690 Franquesa, M., and Albergel, C.: Building a small fire database for Sub-Saharan Africa from Sentinel-2 high-resolution images,
691 Sci. Total Environ., 845, 157139, https://doi.org/10.1016/j.scitotenv.2022.157139, 2022.
692
693 Cochran, W. G.: Sampling techniques. John Wiley & Sons, Hoboken, New Jersey, United States of America, 448pp., ISBN:
694 978-0-471-16240-7, 1977.
695
696 Fernandes, P.: Variation in the Canadian Fire Weather Index Thresholds for Increasingly Larger Fires in Portugal, Forests, 10,
697 838, https://doi.org/10.3390/f10100838, 2019.
698
699 Fernández-García, V., Santamarta, M., Fernández-Manso, A., Quintano, C., Marcos, E., and Calvo, L.: Burn severity metrics
700 in fire-prone pine ecosystems along a climatic gradient using Landsat imagery, Remote Sens. Environ., 206, 205–217,
701 https://doi.org/10.1016/j.rse.2017.12.029, 2018.
702
703 Fernández-García, V., Marcos, E., Fulé, P. Z., Reyes, O., and Santana, V. M.: Fire regimes shape diversity and traits of
704 vegetation under different climatic conditions. Sci. Total Environ., 716, 137137.
705 https://doi.org/10.1016/j.scitotenv.2020.137137, 2020
706

Fernández-García, V. and Alonso-González, E.: Global Patterns and Dynamics of Burned Area and Burn Severity, Remote Sens., 15, 3401, https://doi.org/10.3390/rs15133401, 2023.

Fernández-García, V. and Kull, C. A.: Refining historical burned area data from satellite observations, Int. J. Appl. Earth Obs. Geoinf., 120, 103350, https://doi.org/10.1016/j.jag.2023.103350, 2023.

Fernández-García, V., Franquesa, M., Kull, C. A.: A burned area database from Sentinel-2 imagery (2016-2022) for Madagascar, southern Mozambique, Eswatini and eastern South Africa (Version v1), Zenodo. https://doi.org/10.5281/zenodo.8201841, 2023.

Franquesa, M., Vanderhoof, M. K., Stavrakoudis, D., Gitas, I. Z., Roteta, E., Padilla, M., and Chuvieco, E.: Development of a standard database of reference sites for validating global burned area products, Earth Syst. Sci. Data, 12, 3229–3246, https://doi.org/10.5194/essd-12-3229-2020, 2020.

Franquesa, M., Stehman, S. V., and Chuvieco, E.: Assessment and characterization of sources of error impacting the accuracy of global burned area products, Remote Sens. Environ., 280, 113214, https://doi.org/10.1016/j.rse.2022.113214, 2022a.

Franquesa, M., Lizundia-Loiola, J., Stehman, S. V., and Chuvieco, E.: Using long temporal reference units to assess the spatial accuracy of global satellite-derived burned area products, Remote Sens. Environ., 269, 112823, https://doi.org/10.1016/j.rse.2021.112823, 2022b.

Franquesa, M., Kull, C.A., Fernández-García, V. MGBAS2 reference data: reference fire perimeters obtained from Sentinel-2 imagery over Madagascar for the years 2019 and 2021, e-cienciaDatos, V1, https://doi.org/10.21950/YYZNNN, 2023.

Frappier-Brinton, T. and Lehman, S. M.: The burning island: Spatiotemporal patterns of fire occurrence in Madagascar, edited by: Wan, J.-Z., PLoS ONE, 17, e0263313, https://doi.org/10.1371/journal.pone.0263313, 2022.

Gaveau, D. L. A., Descals, A., Salim, M. A., Sheil, D., and Sloan, S.: Refined burned-area mapping protocol using Sentinel-2 data increases estimate of 2019 Indonesian burning, Earth Syst. Sci. Data, 13, 5353–5368, https://doi.org/10.5194/essd-13-5353-2021, 2021.

Giglio, L., Boschetti, L., Roy, D. P., Humber, M. L., and Justice, C. O.: The Collection 6 MODIS burned area mapping algorithm and product, Remote Sens. Environ., 217, 72–85, https://doi.org/10.1016/j.rse.2018.08.005, 2018.

Goodman, S. M. (Ed.): The New Natural History of Madagascar (2-Volume Set), Princeton University Press, Princeton, New Jersey, United States of America, 2246 pp., ISBN: 9780691222622, 2022a.

Hansen, M. C., Potapov, P. V., Pickens, A. H., Tyukavina, A., Hernandez-Serna, A., Zalles, V., Turubanova, S., Kommareddy, I., Stehman, S. V., Song, X.-P., and Kommareddy, A.: Global land use extent and dispersion within natural land cover using Landsat data, Environ. Res. Lett., 17, 034050, https://doi.org/10.1088/1748-9326/ac46ec, 2022.

Hawbaker, T. J., Vanderhoof, M. K., Schmidt, G. L., Beal, Y.-J., Picotte, J. J., Takacs, J. D., Falgout, J. T., and Dwyer, J. L.: The Landsat Burned Area algorithm and products for the conterminous United States, Remote Sens. Environ., 244, 111801, https://doi.org/10.1016/j.rse.2020.111801, 2020.

Ju, J. and Roy, D. P.: The availability of cloud-free Landsat ETM+ data over the conterminous United States and globally, Remote Sens. Environ., 112, 1196–1211, https://doi.org/10.1016/j.rse.2007.08.011, 2008.

Jones, M. W., Santín, C., van der Werf, G. R., and Doerr, S. H.: Global fire emissions buffered by the production of pyrogenic carbon, Nat. Geosci., 12, 742–747, https://doi.org/10.1038/s41561-019-0403-x, 2019.

Kelly, L. T., Giljohann, K. M., Duane, A., Aquilué, N., Archibald, S., Batllori, E., Bennett, A. F., Buckland, S. T., Canelles, Q., Clarke, M. F., Fortin, M.-J., Hermoso, V., Herrando, S., Keane, R. E., Lake, F. K., McCarthy, M. A., Morán-Ordóñez, A., Parr, C. L., Pausas, J. G., Penman, T. D., Regos, A., Rumpff, L., Santos, J. L., Smith, A. L., Syphard, A. D., Tingley, M. W., and Brotons, L.: Fire and biodiversity in the Anthropocene, Science, 370, https://doi.org/10.1126/science.abb0355, 2020.

Kull, C. A.: Madagascar's Burning Issue: The Persistent Conflict over Fire, Environment: Science and Policy for Sustainable Development, 44, 8–19, https://doi.org/10.1080/00139150209605604, 2002.

Kull, C. A. (Ed.): Isle of Fire: The Political Ecology of Landscape Burning in Madagascar, University of Chicago Press, Chicago, Illinois, United States of America, 256pp., ISBN: 0226461416, 2004.

Liu, M. and Yang, L.: A global fire emission dataset using the three-corner hat method (FiTCH), Earth Syst. Sci. Data Discuss. [preprint], https://doi.org/10.5194/essd-2023-150, in review, 2023.

Lasslop, G., Coppola, A. I., Voulgarakis, A., Yue, C., and Veraverbeke, S.: Influence of Fire on the Carbon Cycle and Climate, Curr. Clim. Change Rep., 5, 112–123, https://doi.org/10.1007/s40641-019-00128-9, 2019.

Liu, S., Zheng, Y., Dalponte, M., and Tong, X.: A novel fire index-based burned area change detection approach using Landsat-8 OLI data, Eur. J. Remote Sens., 53, 104–112, https://doi.org/10.1080/22797254.2020.1738900, 2020.

Lizundia-Loiola, J., Otón, G., Ramo, R., and Chuvieco, E.: A spatio-temporal active-fire clustering approach for global burned area mapping at 250 m from MODIS data, Remote Sens. Environ., 236, 111493, https://doi.org/10.1016/j.rse.2019.111493, 2020.

Lizundia-Loiola, J., Franquesa, M., Boettcher, M., Kirches, G., Pettinari, M. L., and Chuvieco, E.: Implementation of the Burned Area Component of the Copernicus Climate Change Service: From MODIS to OLCI Data, Remote Sens., 13, 4295, https://doi.org/10.3390/rs13214295, 2021.

Lizundia-Loiola, J., Franquesa, M., Khairoun, A., and Chuvieco, E.: Global burned area mapping from Sentinel-3 Synergy and VIIRS active fires, Remote Sens. Environ., 282, 113298, https://doi.org/10.1016/j.rse.2022.113298, 2022.

Long, T., Zhang, Z., He, G., Jiao, W., Tang, C., Wu, B., Zhang, X., Wang, G., and Yin, R.: 30 m Resolution Global Annual Burned Area Mapping Based on Landsat Images and Google Earth Engine, Remote Sens., 11, 489, https://doi.org/10.3390/rs11050489, 2019.

Long T., Zhang Z., He G.: 30 m Resolution Global Annual Burned Area Product, Harvard Dataverse, V1, https://doi.org/10.7910/DVN/3CTMKP, 2021.

Mahood, A. L., Lindrooth, E. J., Cook, M. C., and Balch, J. K.: Country-level fire perimeter datasets (2001–2021), Sci. Data, 9, https://doi.org/10.1038/s41597-022-01572-3, 2022.

Martin, D. A.: Linking fire and the United Nations Sustainable Development Goals, Sci. Total Environ., 662, 547–558, https://doi.org/10.1016/j.scitotenv.2018.12.393, 2019.

Melchiorre, A. and Boschetti, L.: Global Analysis of Burned Area Persistence Time with MODIS Data, Remote Sens., 10, 750, https://doi.org/10.3390/rs10050750, 2018.

Miranda, A., Mentler, R., Moletto-Lobos, Í., Alfaro, G., Aliaga, L., Balbontín, D., Barraza, M., Baumbach, S., Calderón, P., Cárdenas, F., Castillo, I., Contreras, G., de la Barra, F., Galleguillos, M., González, M. E., Hormazábal, C., Lara, A., Mancilla, I., Muñoz, F., Oyarce, C., Pantoja, F., Ramírez, R., and Urrutia, V.: The Landscape Fire Scars Database: mapping historical burned area and fire severity in Chile, Earth Syst. Sci. Data, 14, 3599–3613, https://doi.org/10.5194/essd-14-3599-2022, 2022.

Neves, A. K., Campagnolo, M. L., Silva, J. M. N., and Pereira, J. M. C.: A Landsat-based atlas of monthly burned area for Portugal, 1984–2021, Int. J. Appl. Earth Obs. Geoinf., 119, 103321, https://doi.org/10.1016/j.jag.2023.103321, 2023.

Olofsson, P., Foody, G. M., Herold, M., Stehman, S. V., Woodcock, C. E., and Wulder, M. A.: Good practices for estimating area and assessing accuracy of land change, Remote Sens. Environ., 148, 42–57, https://doi.org/10.1016/j.rse.2014.02.015, 2014.

Olson, D. M., Dinerstein, E., Wikramanayake, E. D., Burgess, N. D., Powell, G. V. N., Underwood, E. C., D'amico, J. A., Itoua, I., Strand, H. E., Morrison, J. C., Loucks, C. J., Allnutt, T. F., Ricketts, T. H., Kura, Y., Lamoreux, J. F., Wettengel, W. W., Hedao, P., and Kassem, K. R.: Terrestrial Ecoregions of the World: A New Map of Life on Earth, BioScience, 51, 933, https://doi.org/10.1641/0006-3568(2001)051[0933:teotwa]2.0.co;2, 2001.

Omisore, A. G.: Attaining Sustainable Development Goals in sub-Saharan Africa; The need to address environmental challenges, Environ. Dev., 25, 138–145, https://doi.org/10.1016/j.envdev.2017.09.002, 2018.

Padilla, M., Stehman, S. V., and Chuvieco, E.: Validation of the 2008 MODIS-MCD45 global burned area product using stratified random sampling, Remote Sens. Environ., 144, 187–196, https://doi.org/10.1016/j.rse.2014.01.008, 2014.

Padilla, M., Stehman, S. V., Ramo, R., Corti, D., Hantson, S., Oliva, P., Alonso-Canas, I., Bradley, A. V., Tansey, K., Mota, B., Pereira, J. M., and Chuvieco, E.: Comparing the accuracies of remote sensing global burned area products using stratified random sampling and estimation, Remote Sens. Environ., 160, 114–121, https://doi.org/10.1016/j.rse.2015.01.005, 2015.

Pereira, P., Brevik, E., Trevisani, S.: Mapping the environment. Sci. Total Environ. 610–611, 17-23. https://doi.org/10.1016/j.scitotenv.2017.08.001, 2018

Phelps, L. N., Andela, N., Gravey, M., Davis, D. S., Kull, C. A., Douglass, K., and Lehmann, C. E. R.: Madagascar's fire regimes challenge global assumptions about landscape degradation, Global Change Biol., 28, 6944–6960, https://doi.org/10.1111/gcb.16206, 2022.

Pullabhotla, H. K., Zahid, M., Heft-Neal, S., Rathi, V., & Burke, M.: Global biomass fires and infant mortality. Proc. Natl. Acad. Sci. U.S.A. 120, e2218210120. https://doi.org/10.1073/pnas.2218210120, 2023.

Quintano, C., Shimabukuro, Y. E., Fernández, A., and Delgado, J. A.: A spectral unmixing approach for mapping burned areas in Mediterranean countries, Int. J. Remote Sens., 26, 1493–1498, https://doi.org/10.1080/01431160412331330220, 2005.

Quintano, C., Fernández-Manso, A., and Fernández-Manso, O.: Combination of Landsat and Sentinel-2 MSI data for initial assessing of burn severity, Int. J. Appl. Earth Obs. Geoinf., 64, 221–225, https://doi.org/10.1016/j.jag.2017.09.014, 2018.

Ralimanana, H., Perrigo, A. L., Smith, R. J., Borrell, J. S., Faurby, S., Rajaonah, M. T., Randriamboavonjy, T., Vorontsova, M. S., Cooke, R. S. C., Phelps, L. N., Sayol, F., Andela, N., Andermann, T., Andriamanohera, A. M., Andriambololonera, S., Bachman, S. P., Bacon, C. D., Baker, W. J., Belluardo, F., Birkinshaw, C., Cable, S., Canales, N. A., Carrillo, J. D., Clegg, R., Clubbe, C., Crottini, A., Damasco, G., Dhanda, S., Edler, D., Farooq, H., de Lima Ferreira, P., Fisher, B. L., Forest, F., Gardiner, L. M., Goodman, S. M., Grace, O. M., Guedes, T. B., Hackel, J., Henniges, M. C., Hill, R., Lehmann, C. E. R., Lowry, P. P., II, Marline, L., Matos-Maraví, P., Moat, J., Neves, B., Nogueira, M. G. C., Onstein, R. E., Papadopulos, A. S. T., Perez-Escobar, O. A., Phillipson, P. B., Pironon, S., Przelomska, N. A. S., Rabarimanarivo, M., Rabehevitra, D., Raharimampionona, J., Rajaonary, F., Rajaovelona, L. R., Rakotoarinivo, M., Rakotoarisoa, A. A., Rakotoarisoa, S. E., Rakotomalala, H. N., Rakotonasolo, F., Ralaiveloarisoa, B. A., Ramirez-Herranz, M., Randriamamonjy, J. E. N., Randrianasolo, V., Rasolohery, A., Ratsifandrihamanana, A. N., Ravololomanana, N., Razafiniary, V., Razanajatovo, H., Razanatsoa, E., Rivers, M., Silvestro, D., Testo, W., Torres Jiménez, M. F., Walker, K., Walker, B. E., Wilkin, P., Williams, J., Ziegler, T., Zizka, A., and Antonelli, A.: Madagascar's extraordinary biodiversity: Threats and opportunities, Science, 378, https://doi.org/10.1126/science.adf1466, 2022.

Ramo, R., Roteta, E., Bistinas, I., van Wees, D., Bastarrika, A., Chuvieco, E., and van der Werf, G. R.: African burned area and fire carbon emissions are strongly impacted by small fires undetected by coarse resolution satellite data, Proc. Natl. Acad. Sci. U.S.A., 118, https://doi.org/10.1073/pnas.2011160118, 2021.

Roberts, G. and Wooster, M. J.: Global impact of landscape fire emissions on surface level PM2.5 concentrations, air quality exposure and population mortality, Atmos. Environ., 252, 118210, https://doi.org/10.1016/j.atmosenv.2021.118210, 2021.

Roteta, E., Bastarrika, A., Padilla, M., Storm, T., and Chuvieco, E.: Development of a Sentinel-2 burned area algorithm: Generation of a small fire database for sub-Saharan Africa, Remote Sens. Environ., 222, 1–17, https://doi.org/10.1016/j.rse.2018.12.011, 2019.

Roteta, E., Bastarrika, A., Franquesa, M., and Chuvieco, E.: A Landsat and Sentinel-2 Based Burned Area Mapping Tools in Google Earth Engine, Remote Sens., 13, 816, https://doi.org/10.3390/rs13040816, 2021a.

Roteta, E., Bastarrika, A., Ibisate, A., and Chuvieco, E.: A Preliminary Global Automatic Burned-Area Algorithm at Medium Resolution in Google Earth Engine, Remote Sens., 13, 4298, https://doi.org/10.3390/rs13214298, 2021b.

Roy, D. P., Boschetti, L., Justice, C. O., and Ju, J.: The collection 5 MODIS burned area product — Global evaluation by comparison with the MODIS active fire product, Remote Sens. Environ., 112, 3690–3707, https://doi.org/10.1016/j.rse.2008.05.013, 2008.

Roy, D. P., Huang, H., Boschetti, L., Giglio, L., Yan, L., Zhang, H. H., and Li, Z.: Landsat-8 and Sentinel-2 burned area mapping - A combined sensor multi-temporal change detection approach, Remote Sens. Environ., 231, 111254, https://doi.org/10.1016/j.rse.2019.111254, 2019.

Sali, M., Piaser, E., Boschetti, M., Brivio, P. A., Sona, G., Bordogna, G., and Stroppiana, D.: A Burned Area Mapping Algorithm for Sentinel-2 Data Based on Approximate Reasoning and Region Growing, Remote Sens., 13, 2214, https://doi.org/10.3390/rs13112214, 2021.

Scales, I. R.: Farming at the Forest Frontier: Land Use and Landscape Change in Western Madagascar, 1896-2005, Environ. Hist., 17, 499–524, https://doi.org/10.3197/096734011x13150366551481, 2011.

Sentinel-2 MSI User Guide: https://sentinels.copernicus.eu/web/sentinel/technical-guides/sentinel-2-msi/msi-instrument, last access: 24 July 2023.

Solofondranohatra, C. L., Vorontsova, M. S., Hempson, G. P., Hackel, J., Cable, S., Vololoniaina, J., and Lehmann, C. E. R.: Fire and grazing determined grasslands of central Madagascar represent ancient assemblages, Proc. R. Soc. B., 287, 20200598, https://doi.org/10.1098/rspb.2020.0598, 2020.

Stroppiana, D., Sali, M., Busetto, L., Boschetti, M., Ranghetti, L., Franquesa, M., Pettinari, M.L., Chuvico, E. Sentinel-2 sampling design and reference fire perimeters to assess accuracy of Burned Area products over Sub-Saharan Africa for the year 2019. ISPRS J. Photogramm. Remote Sens., 191, 223–234, https://doi.org/10.1016/j.isprsjprs.2022.07.015, 2022.

Sudmanns, M., Tiede, D., Augustin, H., and Lang, S.: Assessing global Sentinel-2 coverage dynamics and data availability for operational Earth observation (EO) applications using the EO-Compass, Int. J. Digit. Earth, 13, 768–784, https://doi.org/10.1080/17538947.2019.1572799, 2019.

Tanase, M. A., Kennedy, R., and Aponte, C.: Fire severity estimation from space: a comparison of active and passive sensors and their synergy for different forest types, Int. J. Wildland Fire, 24, 1062, https://doi.org/10.1071/wf15059, 2015.

van der Werf, G. R., Randerson, J. T., Giglio, L., van Leeuwen, T. T., Chen, Y., Rogers, B. M., Mu, M., van Marle, M. J. E., Morton, D. C., Collatz, G. J., Yokelson, R. J., and Kasibhatla, P. S.: Global fire emissions estimates during 1997–2016, Earth Syst. Sci. Data, 9, 697–720, https://doi.org/10.5194/essd-9-697-2017, 2017.

Waeber, P. O., Wilmé, L., Ramamonjisoa, B., Garcia, C., Rakotomalala, D., Rabemananjara, Z. H., Kull, C. A., Ganzhorn, J. U., and Sorg, J.-P.: Dry forests in Madagascar: neglected and under pressure, Int. Forest. Rev., 17, 127–148, https://doi.org/10.1505/146554815815834822, 2015.